Z. Phys. D – Atoms, Molecules and Clusters 6, 163–183 (1987)

489

Atoms, Molecules
Zeitschrift für Physik D and Clusters

Analysis of Collisional Alignment and Orientation Studied by Scattering of Spin-Polarized Electrons from Laser Excited Atoms*

I.V. Hertel, M.H. Kelley, and J.J. McClelland**
Radiation Physics Division, National Bureau of Standards, Gaithersburg, Maryland, USA

Received March 17, 1987

A general framework using density matrices is developed for the analysis of atomic excitation by spin-polarized electrons. This framework is applied to the specific case of the $3S_{1/2} \rightarrow 3P_{3/2}$ transition in Na, as studied by the time-reversed, superelastic process. The scattering is characterized in terms of physical parameters describing the collisionally excited p-state, i.e., its angular momentum ($L_\perp$), linear polarization (P_{lin}), and alignment angle (γ), with these parameters defined separately for singlet and triplet excitation. An expression for the scattering intensity is derived which is valid for arbitrary electron polarization and atomic state preparation. Specific examples are discussed with a view toward complete determination of the relevant scattering amplitudes and phases. Recent experimental results are reevaluated for comparison with theoretical calculations, and suggestions are made for future experiments.

PACS: 34.80.Nz; 34.80.Qb

1. Introduction

Our understanding of electron impact excitation of atoms has substantially matured during recent years. In addition to providing reliable total and differential cross section data for a large variety of atoms, sophisticated experimental techniques are now available for revealing highly instructive details of the collisional process. These include the shape and the inherent angular momentum of the excited atoms after the excitation process, measured as a function of incident electron kinetic energy and scattering angle. In recent years a wealth of data has been obtained in these so-called collisional alignment and orientation studies, notably for $ns \rightarrow n'p$ transitions [1]. Such information may be obtained by detecting the scattered electron at a well defined scattering angle and energy (thereby defining a scattering plane) and in coincidence with it the photon reemitted from the excited atom [2], whereby the polarization and/or angular distribution of the photon provides the information on the magnetic substate population of the collisionally excited atom. Alternatively, one may study the reverse process, $n'p \rightarrow ns$, via superelastic scattering, i.e. prepare an excited atomic target in a well defined mixture of $n'p$ substates by laser optical pumping and observe the differential electron scattering signal for the deexcitation of this atom as a function of the polarization of the exciting laser [3]. In both cases the same information on the relevant scattering amplitudes for the $ns \leftrightarrow n'p$ transition is determined and may be compared with advanced theoretical computations of these parameters.

In spite of the significant progress made during the last years, and sometimes good to excellent agreement between theory and experiment, these studies do reveal a great deal of shortcomings in essentially all the current theories at intermediate energies and larger scattering angles. This situation exists even for seemingly the most simple model cases such as electron impact excitation of helium and atomic hydro-

* Research supported in part by the U.S. Department of Energy. Office of Basic Energy Sciences, Division of Chemical Physics
** Joint Institute for Laboratory Astrophysics, University of Colorado and National Bureau of Standards, Boulder, CO 80309, USA
Permanent Address: Fakultät für Physik, Universität Freiburg, Hermann Herderstrasse 3, D-7800 Freiburg, Federal Republic of Germany

gen [4, 5]. In fact a comparison of experimental and theoretical alignment and orientation parameters, at say 50 eV, leaves us with an almost arbitrary choice of an appropriate theory for scattering angles beyond 90°. It has been argued that this might indicate a general inadequacy of the theoretical approaches in treating a significant contribution of the interaction such as the exchange part of the scattering process. It is obvious that such a shortcoming would deserve the highest attention. Even though the alignment and orientation parameters have been called esoteric [5], they are an excellent tool to amplify specific problems in the theory of electron scattering. Thus they can often lead the way to a greater reliability and general applicability of such calculations to the less esoteric and more integrated quantities such as the differential cross section where one cannot be content with the present state of affairs [5].

Traditionally, the role of electron exchange is clarified by measurements with spin-polarized electrons and spin-polarized targets, perhaps employing spin analysis after the collision process [6, 7]. This approach has seen some success in elastic scattering, to the point that one was able to speak about the "perfect" scattering experiment [8], implying that all theoretically calculable amplitudes could, in principle, be determined by the experiment. However, when Bederson first introduced this concept, it was highly questionable whether one might apply it ever to the inelastic processes as well, since that necessitates the simultaneous application of electron spin selective techniques and the alignment and orientation measurements described above. Since then, vast improvements of the experimental methods in preparing spin-polarized electrons have made such experiments feasible and the first successful differential electron impact excitation study with spin-polarized electrons *and* alignment and orientation analysis was performed by Kessler, Hanne and collaborators [9] for the $e-Hg$ case at forward scattering, a rather complex situation since both electron exchange and spin-orbit interaction are of importance there. A first study with spin analysis after collision from laser excited Na was demonstrated even earlier by Hanne et al. [10], but only most recently a series of first systematic studies for the superelastic scattering of polarized electrons from laser excited Na (3^2P) atoms was reported by McClelland et al. [11, 12]. This system may still be considered a relatively simple model case, being essentially a two electron system, in which spin exchange is the dominant spin dependent interaction which enters into the dynamics of the collision process. Thus the information on alignment and orientation parameters, separated into direct and exchange contributions, seems accessible now and one wants to understand how to make best use of these extraordinary possibilities.

It is the aim of the present paper to provide the general theoretical framework for analyzing experimental studies of superelastic (or inelastic) $np \rightarrow n's$ transitions induced by spin-polarized electrons in laser excited atoms and to illustrate the results with published experimental data. The same analysis would then apply to the reverse process, i.e. the study of an $ns \rightarrow n'p$ transition in an electron-photon coincidence experiment with analysis of the electron and photon polarization.

The following criteria will guide our analysis:

a) We want to evaluate the experimental data in terms of a set of instructive parameters which can be compared with theoretical results, if possible, in such a way that the role of exchange and direct scattering can be separated.

b) We want to disentangle dynamic parameters which describe the collision process from geometrical factors which describe a specific experimental situation. This approach is obviously much more fundamental than merely comparing theoretical results to sets of experimental data for a specific geometry.

c) We want to describe the parameters which can be measured in principle and the most appropriate experimental conditions for the determination of these parameters.

d) The framework to be provided should be connected with the language presently used in alignment and orientation studies without spin analysis and should easily lend itself to be expanded for more complex cases.

We will restrict ourselves here to light atoms where the spin-orbit interaction can be neglected. Furthermore, rather than describing a general atom and arbitrary transition we will be guided by the actual experimental example

$$\mathrm{Na}(^3P_{3/2}\,F=3)+e^- \rightarrow \mathrm{Na}(3^2S_{1/2})+e^- +2.1\ \mathrm{eV} \qquad (1)$$

for which detailed studies with unpolarized electrons are available [13, 14] and which now [11, 12] has been studied by scattering electrons of a well known spin polarization.

The formalism for achieving the above specified goals will be derived by following the spirit of Fano and Macek [15] who developed the necessary framework for analyzing alignment and orientation coincidence studies without spin analysis and which later on was applied to scattering from laser excited atoms [16], again without spin analysis. Advantages and disadvantages of the various sets of parameters for describing standard orientation and alignment studies have been discussed on various occasions [17–19],

and we consider most useful and instructive a set of parameters which directly describes the shape and angular momentum of the atomic p-type charge cloud after the $ns \rightarrow n'p$ collisional excitation process, the time reverse of the system actually studied in the experiment under discussion.

This set of parameters, as specified in [19], consists of $L_\perp$, the angular momentum transferred perpendicular to the scattering plane, γ, the alignment angle of the charge cloud, and P_{lin}, the so-called linear polarization of the charge cloud, i.e. the relative difference between its length and width in the scattering plane. These quantities relate in a very simple way to the density matrix describing the collisionally excited atom in a coordinate frame whose z-axis is perpendicular to the collision plane, the so-called natural frame, in contrast to the usually adopted collision frame whose axis is parallel to the incoming electron beam.

It will be shown in the present work that, with the inclusion of electron spin-polarization, one can introduce and experimentally determine analogous quantities independently for singlet and triplet scattering. Two additional quantities will be introduced, namely the ratio of cross sections for singlet and triplet scattering, and a phase difference between single and triplet amplitudes. The cross-section ratio is measurable in the types of studies discussed here, but the singlet-triplet phase difference would require as well the determination of the electron (and/or atom) spin-polarization after scattering. We will also see that not all of the parameters introduced are independent.

The paper will be structured as follows. We will first discuss briefly, in Sect. 2, the density matrix formalism as it is to be applied to this type of study. In Sect. 3 we will introduce the scattering matrix and the parameters used for describing the collisionally excited atom in an $ns \rightarrow n'p$ transition, and more specifically for an experiment with electron spin analysis (Sect. 3a). Then we derive the preparation matrix of the collisional system (electron plus p-atomic target) as determined by the optical pumping and spin selection process which occur prior to the actual collision studied (Sect. 3b). Combination of the state preparation and scattering matrices gives the very instructive Eq. (24) for the scattering intensity in the general case. One must be aware, however, that the scattering matrix and the preparation matrix are generally derived in different coordinate frames, and that one must therefore perform an appropriate frame rotation (Sect. 3c). We do this, in the Appendix, with an irreducible representation of the preparation matrix in terms of real multipole moments. By using standard tensor algebra and the Wigner-Eckart theorem this allows us at the same time to project these quantities from the hyperfine coupling scheme $|(JI)\,FM_F\rangle$, in which the atom is prepared by optical pumping, onto the $|(LS)\,JM_J\rangle$ fine-structure coupling scheme, in which the density matrix is needed for describing the present scattering data. We then discuss, in Sect. 4, some specific examples of experimental geometry and derive formulae to evaluate the scattering signals in terms of the dynamical parameters introduced above (Sects. 4a–d). As a further topic we address relations among the different matrix elements and parameters and discuss the number of measurements necessary to completely characterize the $3P \rightarrow 3S$ transition under study (Sect. 4e). We then present, in Sect. 5, a detailed evaluation of the previously published experimental data [11–13]. Measurements with circularly polarized optical pumping are compared (Sect. 5a) to theoretical results from the literature, namely the 4-state close-coupling calculations of Moores and Norcross [20] and the distorted wave results of Kennedy et al. [21]. As will be seen, the overall agreement between theory and experiment is good only for the lowest energies, while some interesting disagreements are found at relatively higher energies (~ 10.0 eV). Significant conclusions may be drawn individually for the singlet and triplet scattering channels. Some interesting geometrical implications are then discussed in context with the interpretation of measurements with linearly polarized light (Sect. 5b).

2. General Theory of Measurement

In the most general case of state-selected scattering experiments, state selection can be either complete, partial, or nonexistent in any of the available scattering channels. To allow for all of these possibilities, the connection between theory and experiment is most conveniently made in the density matrix formalism. The intensity of particles with a specific incident energy scattered into scattering angle θ_{scat} is given by [22–25]

$$I = \eta \frac{k_f}{k_i} N_f \,\mathrm{Tr}(\boldsymbol{\sigma}^{\text{det}} \mathbf{F} \boldsymbol{\sigma}^{\text{prep}} \mathbf{F}^\dagger). \tag{2}$$

In this expression, the constant η contains all purely experimental factors such as target and projectile densities, detection efficiencies, etc. The initial and scattered projectile momenta are given by k_i and k_f, respectively. The density matrices $\boldsymbol{\sigma}^{\text{det}}$ and $\boldsymbol{\sigma}^{\text{prep}}$ describe the state selection in the detection and preparation processes, respectively, and are assumed normalized such that each has unit trace. The total number of final states detected in the experiment is given by N_f and appears in (2) to compensate for the normaliza-

tion of σ^{det}. All scattering information about transitions from any initial state $|i\rangle$ to any final state $|f\rangle$ of the system is contained in the transition matrix F, whose elements are the complex scattering amplitudes $f_{fi}(\theta_{scat})$ obtained, e.g., from ab initio calculations.

The great advantage of (2) for expressing the scattering intensity is that it separates clearly the various factors which determine the outcome of any measurement, and hence allows one to use a "divide and conquer" approach in the analysis of a rather complex problem. In particular, the contribution from scattering dynamics is contained entirely within **F**, while the details of the initial state preparation or final state detection are contained entirely within σ^{det} or σ^{prep}, respectively. Thus, one can treat each of these contributions independently of the others, in whatever manner is most convenient or appropriate. In addition, careful inspection of the expressions can indicate which specific measurements must be performed to investigate specific aspects of the transition matrix.

The measurements which stimulated the present work utilized preparation of the initial states (spin and/or orbital angular momentum) of each incident particle, but did not include analysis of the final states [11, 12]. Thus we concentrate at present on extending previous treatments of (2) to include explicitly the effects of electron spin exchange in scattering processes that include spin analysis of both collision partners prior to the collision. This allows us to write $\sigma^{det}=\frac{1}{N_f}\mathbf{1}$, after which (2) simplifies to

$$I=C\,\mathrm{Tr}(\mathbf{F}\sigma^{prep}\mathbf{F}^{\dagger})=C\,\mathrm{Tr}(\sigma^{prep}\mathbf{F}^{\dagger}\mathbf{F}) =C\,\mathrm{Tr}(\sigma^{prep}\rho), \tag{3}$$

where the constant C is the product of the experimental efficiency η, and the flux factor $\frac{k_f}{k_i}$. We have also defined the matrix $\rho=\mathbf{F}^{\dagger}\mathbf{F}$ with elements given by

$$\rho_{ii'}=\sum_f f_{fi}^{*}(\theta_{scat})f_{fi'}(\theta_{scat}). \tag{4}$$

In the remainder of this paper, we refer to this matrix ρ as the "scattering matrix".

This scattering matrix ρ is $N_i\times N_i$ Hermitian, where N_i is the number of possible initial states. Because it involves a sum over final states of the system, some information about the scattering will be hidden to the experiment. Even so, we shall see that significantly more information is retained than is available in conventional cross section measurements not utilizing state selection.

While the remainder of this paper treats specifically experiments which employ state selection before but not after the interaction, the approach used is completely valid for treating experiments which use state analysis after the interaction but not before. The crucial point is that one of the state density matrices, either preparation or detection, should be proportional to the unit matrix, so that one need treat only the matrix product of the transition matrix and its adjoint. It should be noted, in fact, that the scattering matrix derived from (3) is precisely the scattering matrix one would use in the time-reversed experiment, i.e. inelastic coincidence measurements in which one does no preparation of the initial ground states, but does detect the spin of the scattered electron and/or the state of the excited atom.

Some treatments of this inelastic process have used a different normalization for the scattering matrix, requiring that it have unit trace [13, 17, 19]. We have chosen for reasons of clarity in several expressions to be derived, however, to normalize such that the trace is proportional to the spin averaged differential scattering cross section, $\left.\frac{d\sigma}{d\Omega}\right|_{i\to f}$, for the forward scattering process $i\to f$. Specifically,

$$\mathrm{Tr}(\rho)=Q_0(\theta_{scat})=\frac{k_i}{k_f}N_i\left.\frac{d\sigma}{d\Omega}\right|_{i\to f}. \tag{5}$$

Throughout the remainder of this paper, Q_0 will be used to denote this angle dependent normalization[1]. The degeneracy factors are $N_i=3\cdot4=12$ and $N_f=4$ for the case under study with three degenerate $3p$ orbitals and four possible states for the two incident electron spins.

3. Theory of Spin-Polarized Superelastic Scattering from Na($3^2P_{3/2}$)

The expression (3) for the scattering intensity is the central relation of the rest of this paper, in which we will be discussing its explicit evaluation for the case of spin-polarized electron scattering from optically pumped Na($3^2P_{3/2}$). A key step in the explicit evaluation of (3) is the choice of coordinate system and basis states with which to represent the matrices

[1] Note that this normalization is independent of whether one is describing an $np\to n's$ transition superelastically, or an $ns\to n'p$ transition inelastically. We have defined everything in terms of the actual initial and final states. While the inelastic differential cross section differs from the superelastic cross section, due to the flux and degeneracy factor, the normalization of the scattering matrix, Q_0, is exactly the same in each case. With this normalization, the scattering matrix is analogous to a "differential collision strength"

σ and ρ. While this choice is in a sense arbitrary, a judicious choice at the outset reduces both the complexity of the resulting expressions and the work involved in generating them. Furthermore, it can make explicitly clear the connection between various theoretically calculable and experimentally observable quantities. To this end, we first choose to derive expressions for σ and ρ in different basis sets, each of which is chosen according to its appropriateness for the matrix in question. Then, for evaluation of the experimental intensity, each matrix is re-expressed in terms of a third, common, set of basis states. This third set is chosen both to minimize the complexity of the transformation from each of the original basis sets, and also to express most simply the experimental conditions. While this approach may seem at first glance unduly involved, it will be seen that it is the "path of least resistance", in that the expressions so derived are relatively simple and accurately reproduce the symmetries inherent in the physics of the scattering process.

3a. *The Scattering Matrix*

We begin by writing an expression for the scattering matrix in its most appropriate basis. For the present work we are specifically interested in limiting our investigations to the role played by spin exchange in low energy collisions with light atoms. Within this limitation, we can make several reasonable assumptions about the scattering dynamics which greatly reduce the complexity of theoretical expressions. First, we assume that the nonzero nuclear spin plays no dynamic role during the relatively short duration of the collision. Further, we assume that the spins of both the scattered and atomic electrons remain uncoupled from the atomic orbital angular momentum during the collision, but couple to each other to form a composite spin $\mathscr{S}$. These together comprise the Percival-Seaton hypothesis [26], and allow us to completely describe the effect of the nuclear spin through angular momentum recoupling coefficients. Finally, we choose to neglect the continuum spin-orbit interaction so that $\mathscr{S}$ and $\mathscr{M}_{\mathscr{S}}$ are conserved during the collision. For a light target such as sodium, this is a good approximation. Thus we see that a reasonable choice for describing the relevant quantum states of the system is the basis set $|LM_L\mathscr{S}\mathscr{M}_{\mathscr{S}}\rangle$, because in this basis set, the scattering matrix is diagonal in $\mathscr{S}$ and $\mathscr{M}_{\mathscr{S}}$. We therefore introduce scattering sub-matrices, **s** and **t**, for scattering via the singlet and triplet spin states respectively. These are each 3×3 matrices with rows and columns for $M_L=\pm 1, 0$. The scattering matrix ρ can then be written as

$$\rho=\begin{pmatrix} \mathbf{t} & 0 & 0 & 0 \\ 0 & \mathbf{t} & 0 & 0 \\ 0 & 0 & \mathbf{t} & 0 \\ 0 & 0 & 0 & \mathbf{s} \end{pmatrix}, \tag{6}$$

where the rows and columns are labeled by $(\mathscr{S}\mathscr{M}_{\mathscr{S}})$ $=(11), (10), (1\text{-}1)$, and (00).

We now need to consider the elements of the individual matrices **t** and **s**. Owing to the overall positive reflection symmetry about the scattering plane, angular momentum can be transferred only perpendicular to that plane. Consequently, if the quantization axis is chosen normal to the scattering plane, the matrics **t** and **s** take on particularly simple forms, i.e.

$$\mathbf{t}=\begin{pmatrix} t_{11} & 0 & t_{1-1} \\ 0 & 0 & 0 \\ t_{-11} & 0 & t_{-1-1} \end{pmatrix} \tag{7a}$$

and

$$\mathbf{s}=\begin{pmatrix} s_{11} & 0 & s_{1-1} \\ 0 & 0 & 0 \\ s_{-11} & 0 & s_{-1-1} \end{pmatrix}. \tag{7b}$$

One should note that it is only in such a "natural frame" [17] that the scattering matrices take on this simple form. Often, however, scattering amplitudes are given in the so-called "collision frame" in which the z-axis is along the incident electron direction. In such case, one must reexpress those amplitudes in the natural frame prior to use in (7a–b) [17, 18].

It is essential to specify very carefully what frame is chosen as the "natural frame". A reasonable convention would be to choose the $\hat{\mathbf{z}}$-axis parallel to the projectile's (classical) angular momentum, with the $\hat{\mathbf{x}}$ and $\hat{\mathbf{y}}$ axes fixed relative to the incoming direction. Specifically, $\hat{\mathbf{z}}_{\text{nat}}=\hat{\mathbf{k}}_{\text{in}}\times\hat{\mathbf{k}}_{\text{out}}$ and $\hat{\mathbf{x}}_{\text{nat}}=\hat{\mathbf{k}}_{\text{in}}$ would seem to be the most appropriate choice for the coordinate system. We make at present, however, an alternative choice for the "natural frame" in order to emphasize the connection between the superelastic experiments under consideration and the time-reversed, inelastic coincidence studies of the same transition. In particular, we choose $\hat{\mathbf{z}}_{\text{nat}}=-(\hat{\mathbf{k}}_{\text{in}}\times\hat{\mathbf{k}}_{\text{out}})$ and $\hat{\mathbf{x}}_{\text{nat}}=-\hat{\mathbf{k}}_{\text{out}}$. This is precisely the choice of the "natural frame" for the time-reversed process.

With this choice of coordinate system, the scattering amplitudes, $f_{fi}(\theta_{\text{scat}})$, for collisional deexcitation from state $|i\rangle$ to state $|f\rangle$ are merely the complex conjugates of the scattering amplitudes, $f_{if}(\theta_{\text{scat}})$, for collisional excitation from state $|f\rangle$ to state $|i\rangle$. Consequently, the scattering matrix of (4) is precisely the same for either type of experiment. The matrices **s**

and **t** can thus be compared directly with the scattering matrix previously used to describe inelastic experiments using unpolarized electrons [13, 17, 19]. That matrix, ρ_{unpol}, is given by

$$\rho_{\text{unpol}}=\tfrac{1}{2}\begin{pmatrix} 1+L_\perp & 0 & -P_{\text{lin}}\,e^{-2i\gamma} \\ 0 & \rho_{00} & 0 \\ -P_{\text{lin}}\,e^{2i\gamma} & 0 & 1-L_\perp \end{pmatrix} \tag{8}$$

and is related to our present scattering matrix by

$$\rho_{\text{unpol}}=\frac{1}{Q_0}\operatorname*{Tr}_{s,t}\rho \tag{9}$$

where $\operatorname*{Tr}_{s,t}$ indicates summation over the singlet and triplet parts in (6). Thus the matrix elements of ρ_{unpol} are $(3t_{M_L M_L'}+s_{M_L M_L'})/Q_0$.[2]

The four parameters $L_\perp$, P_{lin}, γ and ρ_{00} take their significance from the inelastic $ns\to n'p$ transition. $L_\perp$ is the angular momentum transferred to the atom along $\hat{\mathbf{z}}_{\text{nat}}$, i.e., perpendicular to the scattering plane. P_{lin} is the linear polarization of the charge cloud of the excited p-state; that is, its length minus its width divided by the sum of the two. The angle γ is the alignment angle in the scattering plane of the axis of the charge cloud with respect to the incident electron direction. The parameter ρ_{00}, which describes the "height" of the charge cloud along $\hat{\mathbf{z}}_{\text{nat}}$, vanishes, in the absence of the spin orbit interaction, for a $np\leftrightarrow n's$ transition.

The net effect of introducing spin polarization to the initial state preparation is to double the number of parameters needed to describe the scattering. We therefore introduce, analogously to the spin unpolarized case, the quantities $L_\perp^s$, $L_\perp^t$, P_{lin}^s, P_{lin}^t, γ^s, and γ^t with which to characterize the singlet and triplet scattering matrices. These matrices can then be expressed by

$$\mathbf{s}=\tfrac{1}{2}Q_0^s\begin{pmatrix} 1+L_\perp^s & 0 & -P_{\text{lin}}^s\,e^{-2i\gamma^s} \\ 0 & 0 & 0 \\ -P_{\text{lin}}^s\,e^{2i\gamma^s} & 0 & 1-L_\perp^s \end{pmatrix}, \tag{10a}$$

$$\mathbf{t}=\tfrac{1}{2}Q_0^t\begin{pmatrix} 1+L_\perp^t & 0 & -P_{\text{lin}}^t\,e^{-2i\gamma^t} \\ 0 & 0 & 0 \\ -P_{\text{lin}}^t\,e^{2i\gamma^t} & 0 & 1-L_\perp^t \end{pmatrix}. \tag{10b}$$

[2] Had we strictly adhered to our definition above of the "natural frame", the coordinate system would have had its $\hat{\mathbf{z}}$-axis in the opposite direction and its $\hat{\mathbf{x}}$-axis would have been rotated though an angle $\pi-\theta_{\text{scat}}$ about the $\hat{\mathbf{z}}$-axis. In that frame, the amplitudes, $f_{\pm 1}(\theta_{\text{scat}})$, for collisional deexcitation would have had an additional phase factor, due to the coordinate rotation. Consequently, the off-diagonal elements of the scattering matrices **t** and **s** would have also had an additional phase factor

Here we have introduced Q_0^s and Q_0^t which are proportional to the isotropic part of the partial differential cross section for singlet and triplet scattering, respectively. We note that

$$\begin{aligned} Q_0&=\operatorname{Tr}(\rho)=3\operatorname{Tr}(\mathbf{t})+\operatorname{Tr}(\mathbf{s})=3Q_0^t+Q_0^s \\ &=3(t_{11}+t_{-1-1})+(s_{11}+s_{-1-1})=(3r+1)\,Q_0^s \\ &=\frac{(3r+1)}{r}Q_0^t \end{aligned} \tag{11}$$

where we have defined the cross section ratio, r, as

$$r=\frac{Q_0^t}{Q_0^s}. \tag{12}$$

At this point we note that while the scattering matrix is particularly simple when represented in the $|LM_L\mathcal{S}\mathcal{M}_{\mathcal{S}}\rangle$ basis, a closer connection to possible experiments is achieved if one uncouples the electron and atoms spins and represents the scattering matrix in the $|LM_L SM_S sm_s\rangle$ basis. That is because experimentally one cannot uniquely prepare the singlet or triplet spin states, but one can prepare the spins initially to be either parallel or anti-parallel. The elements of the scattering matrix in the $|LM_L SM_S sm_s\rangle$ representation are related to those in the $|LM_L\mathcal{S}\mathcal{M}_{\mathcal{S}}\rangle$ representation by

$$\begin{aligned} &\rho_{M_S m,M_S' m_s'} \\ &=\sum_{\mathcal{S}\mathcal{M}}\langle SM_S sm_s|\mathcal{S}\mathcal{M}\rangle\langle\mathcal{S}\mathcal{M}|SM_S' sm_s'\rangle\,\rho_{\mathcal{S}\mathcal{M}_{\mathcal{S}},\mathcal{S}\mathcal{M}_{\mathcal{S}}}, \end{aligned} \tag{13}$$

where we have made use of the fact that ρ is diagonal in $\mathcal{S}$ and $\mathcal{M}_{\mathcal{S}}$.

The final form for the scattering matrix ρ is then given by

$$\rho=\begin{pmatrix} \mathbf{t} & 0 & 0 & 0 \\ 0 & \frac{1}{2}(\mathbf{t}+\mathbf{s}) & \frac{1}{2}(\mathbf{t}-\mathbf{s}) & 0 \\ 0 & \frac{1}{2}(\mathbf{t}-\mathbf{s})^\dagger & \frac{1}{2}(\mathbf{t}+\mathbf{s}) & 0 \\ 0 & 0 & 0 & \mathbf{t} \end{pmatrix}, \tag{14}$$

where the rows and columns are labeled by $(M_S, m_s)=(\frac{1}{2},\frac{1}{2}),(\frac{1}{2},-\frac{1}{2}),(-\frac{1}{2},\frac{1}{2})$, and $(-\frac{1}{2},-\frac{1}{2})$.

3b. Preparation Matrix

We now turn our attention to derivation of the matrix σ^{prep} which describes the initial state preparation. We note the preparation matrix must encompass the preparation not only of the atom, but also of the incident electron, since it is polarized prior to collision. Because the electron and atom are considered to be separate systems before the collision, we may

write the combined density matrix as the direct product of individual matrices, σ^{el} and σ^{atom}, for the electron and atom respectively:

$$\sigma^{prep}=\sigma^{atom}\otimes\sigma^{el}. \tag{15}$$

The electron spin density matrix is given by [7]

$$\sigma^{el}=\tfrac{1}{2}\begin{pmatrix}1+P_z & P_x+iP_y\\ P_x-iP_y & 1-P_z\end{pmatrix} \tag{16}$$

where P_x, P_y and P_z are the three components of the electron polarization vector. This electron polarization is expressed in the natural frame to maintain correspondence with the collision matrix derived in the previous section.

The atomic preparation matrix σ^{prep} is obtained by careful consideration of the optical pumping used to create the atomic excited state. The atom is prepared in a distribution of magnetic sublevels of a single hyperfine state by laser optical pumping. The optical pumping is best described in a coordinate system called the "photon frame" [27, 3]. For pumping with circularly polarized light, this frame has the $\hat{\mathbf{z}}$ quantization axis parallel to the propagation direction of the laser. For linearly polarized light, the electric vector of the light determines the z-axis. In the photon frame, the atomic density matrix, expressed in terms of the F-coupled states of the free atom, is a diagonal matrix when linearly of circularly polarized light is used [27].

What is needed for use with the scattering matrix derived in the previous section is the atomic density matrix in the natural frame expressed in terms of the $|LM_L\,SM_S\rangle$ representation. Transformation of the diagonal density matrix into this form involves three steps. First we project the F-coupled density matrix onto the J-coupled basis states, then rotate the matrix from the photon frame into the natural frame, and finally recouple into the $|LM_L\,SM_S\rangle$ representation [27]. Each of these operations can be performed relatively simply using the moments of a multipole expansion of the density matrix [3, 4]. These moments transform in a simple way under coordinate rotations, and the details of the transformations are included in the Appendix. Here we take as a starting point the atomic density matrix in the natural frame in the $|JM_J\rangle$ representation, with the matrix elements expressed in terms of optical pumping parameters determined in the photon frame. The resulting 6×6 matrix has rows and columns labeled by $(JM_J)=(\frac{3}{2},\frac{3}{2})$, $(\frac{3}{2},\frac{1}{2})$, $(\frac{3}{2},-\frac{1}{2})$, $(\frac{3}{2},-\frac{3}{2})$, $(\frac{1}{2},\frac{1}{2})$, and $(\frac{1}{2},-\frac{1}{2})$. The explicit evaluation of the $\sigma_{JM_J,J'M'_J}$ in terms of the photon frame optical pumping parameters is included in the Appendix.

In the previous section, the scattering matrix was finally expressed in the uncoupled $|LM_L\,SM_S\,sm_s\rangle$ basis set. Thus we must derive an expression for the preparation matrix in this representation in terms of the elements $\sigma^{atom}_{JM_J,J'M'_J}$ in the $|JM_J\rangle$ representation. In the new representation, the matrix elements are given by

$$\sigma^{atom}_{M_LM_S,M'_LM'_S}=\sum_{JM_JJ'M'_J}\langle LM_L\,SM_S|JM_J\rangle \cdot\langle J'M'_J|LM'_L\,SM'_S\rangle\,\sigma^{atom}_{JM_J\,J'M'_J} \tag{17a}$$

$$=\langle LM_L\,SM_S|J(M_L+M_S)\rangle \cdot\langle LM'_L\,SM'_S|J(M'_L+M'_S)\rangle \cdot\sigma^{atom}_{J(M_L+M_S),J(M'_L+M'_S)}, \tag{17b}$$

where in the second step we have made use of the selection rules for Clebsch-Gordan coefficients and the fact that, since only a single fine structure level is optically excited, $J=J'$.

This 6×6 matrix $\sigma^{atom}_{M_LM_S,M'_LM'_S}$ is re-expressed in terms of a 2×2 matrix whose elements are each 3×3 submatrices. That is,

$$\sigma^{atom}=\begin{pmatrix}\sigma^{++} & \sigma^{+-}\\ \sigma^{-+} & \sigma^{--}\end{pmatrix} \tag{18}$$

with rows and columns labeled by $+$ and $-$ for $M_S=+\frac{1}{2}$, $-\frac{1}{2}$, respectively. Each of the sub-matrices in (18) has rows and columns labeled by $M_L=+1$, 0, -1. Thus, we have, for example

$$(\sigma^{++})_{M_LM'_L}=\sigma_{M_L\frac{1}{2},M'_L\frac{1}{2}},\ \text{etc.} \tag{19}$$

The four sub-matrices evaluate to

$$\sigma^{++}=\begin{pmatrix}\sigma_{\frac{3}{2},\frac{3}{2}} & \sqrt{\frac{2}{3}}\sigma_{\frac{3}{2},\frac{1}{2}} & \sqrt{\frac{1}{3}}\sigma_{\frac{3}{2},-\frac{1}{2}}\\ \sqrt{\frac{2}{3}}\sigma_{\frac{1}{2},\frac{3}{2}} & \frac{2}{3}\sigma_{\frac{1}{2},\frac{1}{2}} & \frac{\sqrt{2}}{3}\sigma_{\frac{1}{2},-\frac{1}{2}}\\ \sqrt{\frac{1}{3}}\sigma_{-\frac{1}{2},\frac{3}{2}} & \frac{\sqrt{2}}{3}\sigma_{-\frac{1}{2},\frac{1}{2}} & \sigma_{-\frac{1}{2},-\frac{1}{2}}\end{pmatrix}, \tag{20a}$$

$$\sigma^{+-}=(\sigma^{-+})^{\dagger}=\begin{pmatrix}\sqrt{\frac{1}{3}}\sigma_{\frac{3}{2},\frac{1}{2}} & \sqrt{\frac{2}{3}}\sigma_{\frac{3}{2},-\frac{1}{2}} & \sigma_{\frac{3}{2},-\frac{3}{2}}\\ \frac{\sqrt{2}}{3}\sigma_{\frac{1}{2},\frac{1}{2}} & \frac{2}{3}\sigma_{\frac{1}{2},-\frac{1}{2}} & \sqrt{\frac{2}{3}}\sigma_{\frac{1}{2},-\frac{3}{2}}\\ \frac{1}{3}\sigma_{-\frac{1}{2},\frac{1}{2}} & \frac{\sqrt{2}}{3}\sigma_{-\frac{1}{2},-\frac{1}{2}} & \sqrt{\frac{1}{3}}\sigma_{-\frac{1}{2},-\frac{3}{2}}\end{pmatrix} \tag{20b}$$

and finally,

$$\boldsymbol{\sigma}^{--}=\begin{pmatrix} \frac{1}{3}\sigma_{\frac{1}{2},\frac{1}{2}} & \frac{\sqrt{2}}{3}\sigma_{\frac{1}{2},-\frac{1}{2}} & \sqrt{\frac{1}{3}}\sigma_{\frac{1}{2},-\frac{3}{2}} \\ \frac{\sqrt{2}}{3}\sigma_{-\frac{1}{2},\frac{1}{2}} & \frac{2}{3}\sigma_{-\frac{1}{2},-\frac{1}{2}} & \frac{\sqrt{2}}{3}\sigma_{-\frac{1}{2},-\frac{3}{2}} \\ \sqrt{\frac{1}{3}}\sigma_{-\frac{3}{2},\frac{1}{2}} & \frac{\sqrt{2}}{3}\sigma_{-\frac{3}{2},-\frac{1}{2}} & \sigma_{-\frac{3}{2},-\frac{3}{2}} \end{pmatrix}. \tag{20c}$$

The electron spin polarization properties of the atomic density matrix in (18) are made clearer if we rewrite the matrix, in analogy with (16), as

$$\boldsymbol{\sigma}^{\text{atom}}=\tfrac{1}{2}\begin{pmatrix} (\boldsymbol{\sigma}_0+\boldsymbol{\sigma}_z) & (\boldsymbol{\sigma}_x+i\boldsymbol{\sigma}_y) \\ (\boldsymbol{\sigma}_x-i\boldsymbol{\sigma}_y) & (\boldsymbol{\sigma}_0-\boldsymbol{\sigma}_z) \end{pmatrix} \tag{21}$$

with the definitions

$$\boldsymbol{\sigma}_0=(\boldsymbol{\sigma}^{++}+\boldsymbol{\sigma}^{--}), \tag{22a}$$
$$\boldsymbol{\sigma}_x=(\boldsymbol{\sigma}^{-+}+\boldsymbol{\sigma}^{+-}), \tag{22b}$$
$$\boldsymbol{\sigma}_y=i(\boldsymbol{\sigma}^{-+}-\boldsymbol{\sigma}^{+-}), \tag{22c}$$
$$\boldsymbol{\sigma}_z=(\boldsymbol{\sigma}^{++}-\boldsymbol{\sigma}^{--}) \tag{22d}$$

The matrices $\boldsymbol{\sigma}_x$, $\boldsymbol{\sigma}_y$, and $\boldsymbol{\sigma}_z$ are 3×3 matrices describing spin polarization of the atom along the $\hat{\mathbf{x}}$, $\hat{\mathbf{y}}$, and $\hat{\mathbf{z}}$ axes, respectively. The matrix $\boldsymbol{\sigma}_0$ describes the spin-unpolarized part of the density matrix.

Combining (16) and (21), and keeping in mind the definitions from (20a–c), we finally obtain the preparation matrix, in the uncoupled basis, in a form which can be used directly with the scattering matrix from (14):

$$\boldsymbol{\sigma}^{\text{prep}}=\tfrac{1}{4}\begin{pmatrix} (\boldsymbol{\sigma}_0+\boldsymbol{\sigma}_z) & (\boldsymbol{\sigma}_x+i\boldsymbol{\sigma}_y) \\ (\boldsymbol{\sigma}_x-i\boldsymbol{\sigma}_y) & (\boldsymbol{\sigma}_0-\boldsymbol{\sigma}_z) \end{pmatrix}\otimes\begin{pmatrix} (1+P_z) & (P_x+iP_y) \\ (P_x-iP_y) & (1-P_z) \end{pmatrix}. \tag{23}$$

It should be noted that this form of the density matrix, $\boldsymbol{\sigma}^{\text{prep}}$, could equally well describe the density matrix, $\boldsymbol{\sigma}^{\text{det}}$, which describes an inelastic coincidence experiment employing spin-polarization analysis of the scattered electron.

3c. Scattering Intensity

The results of Sects 3a and 3b for the collision and preparation matrices, (14) and (23), allow us to explicitly evaluate (3), which gives the scattering intensity. We obtain

$$I=\frac{C}{4}[\mathrm{Tr}[\boldsymbol{\sigma}_0(3\mathbf{t}+\mathbf{s})]+P_x\,\mathrm{Tr}[\boldsymbol{\sigma}_x(\mathbf{t}-\mathbf{s})] +P_y\,\mathrm{Tr}[\boldsymbol{\sigma}_y(\mathbf{t}-\mathbf{s})]+P_z\,\mathrm{Tr}[\boldsymbol{\sigma}_z(\mathbf{t}-\mathbf{s})]]. \tag{24}$$

Equation (24) contains the basic information needed to make decisions about how best to prepare the atom and electron in order to extract the maximum information about the matrices $\mathbf{t}$ and $\mathbf{s}$. From the first term, we see that with unpolarized electrons, we obtain information about the matrix sum $(3\mathbf{t}+\mathbf{s})$. The addition of electron spin-polarization allows us to determine the matrix difference $(\mathbf{t}-\mathbf{s})$ as well.

The goal is then to determine what optical pumping schemes produce preparation matrices which have diagonal and/or off-diagonal terms so that all elements of the matrices $(3\mathbf{t}+\mathbf{s})$ and $(\mathbf{t}-\mathbf{s})$ can be probed. For the sum, this has essentially been done in previous unpolarized superelastic scattering work by pumping with clockwise and counter-clockwise circularly polarized light, and also with linearly polarized light [3, 4, 13, 17]. For the difference, a spin-polarized experiment is required in order to determine the matrix elements. We note that spin-polarization along any one axis, e.g. the $\hat{\mathbf{z}}$-axis, is sufficient to extract all the information, since the same difference, $\mathbf{t}-\mathbf{s}$, appears in each term. The combination of spin-polarized and unpolarized measurements then gives complete information on the individual singlet and triplet contributions to the scattering, with the exception that nothing is learned about the relative phase between singlet and triplet scattering.

In the remainder of this paper, we will concentrate on obtaining explicit expressions for the matrices $\boldsymbol{\sigma}_0$, $\boldsymbol{\sigma}_x$, $\boldsymbol{\sigma}_y$ and $\boldsymbol{\sigma}_z$ for various specific optical pumping configurations. For use in the following sections, we write down general expressions for these matrices in terms of the optical pumping parameters and the polar angles θ and φ defining the direction of $\hat{\mathbf{z}}_{\text{photon}}$ with respect to the natural frame (see Fig. 8 in the Appendix). The parameters o_0 (orientation), a_0 (alignment) and e_0 (octopole moment) are defined in the Appendix, and are the only three parameters necessary to describe the atom if pure linear or circular polarization is used. In order to obtain the expressions shown below, we have first combined (A 7a–c) and (A 10a–c) from the Appendix to get natural frame real multipole moments. Then we have used (A 6a–j) to get expressions for $\sigma_{M_J M_J'}$ which are subsequently inserted into (20, 22) to obtain the results for $\boldsymbol{\sigma}_0$, $\boldsymbol{\sigma}_x$, $\boldsymbol{\sigma}_y$, and $\boldsymbol{\sigma}_z$. In the interest of simplicity, we have omitted the rows and columns corresponding to $M_L=0$ because they are all zero. We thus obtain

$$\boldsymbol{\sigma}_0=\tfrac{1}{3}\begin{pmatrix}1+o_0\cos\theta+\frac{1}{12}a_0(3\cos^2\theta-1) & \frac{1}{4}a_0\sin^2\theta\,e^{-2i\varphi}\\ \text{C.C.} & 1-o_0\cos\theta+\frac{1}{12}a_0(3\cos^2\theta-1)\end{pmatrix} \tag{25a}$$

$$\boldsymbol{\sigma}_x=\frac{\sin\theta}{3}\begin{pmatrix}\cos\varphi\left[\frac{3}{5}o_0+\frac{1}{2}a_0\cos\theta+\frac{1}{30}e_0(5\cos^2\theta-1)\right] & e_0\left[\frac{1}{12}\sin^2\theta\,e^{-3i\varphi}\right.\\ & \left.\frac{1}{60}(1-5\cos^2\theta)\,e^{-i\varphi}\right]+o_0\frac{1}{5}e^{-i\varphi}\\ \text{C.C.} & \cos\varphi\left[\frac{3}{5}o_0-\frac{1}{2}a_0\cos\theta+\frac{1}{30}e_0(5\cos^2\theta-1)\right]\end{pmatrix}, \tag{25b}$$

$$\boldsymbol{\sigma}_y=\frac{\sin\theta}{3}\begin{pmatrix}\sin\varphi\left[\frac{3}{5}o_0+\frac{1}{2}a_0\cos\theta+\frac{1}{30}e_0(5\cos^2\theta-1)\right] & -ie_0\left[\frac{1}{12}\sin^2\theta\,e^{-3i\varphi}-\right.\\ & \left.\frac{1}{60}(1-5\cos^2\theta)\,e^{-i\varphi}\right]+\frac{i}{5}o_0\,e^{-i\varphi}\\ \text{C.C.} & \sin\varphi\left[\frac{3}{5}o_0-\frac{1}{2}a_0\cos\theta+\frac{1}{30}e_0(5\cos^2\theta-1)\right]\end{pmatrix}, \tag{25c}$$

$$\boldsymbol{\sigma}_z=\tfrac{1}{3}\begin{pmatrix}\frac{1}{2}+\frac{4}{5}o_0\cos\theta+\frac{1}{6}a_0(3\cos^2\theta-1)+\frac{1}{30}e_0(5\cos^3\theta-3\cos\theta) & \frac{1}{6}e_0\sin^2\theta\cos\theta\,e^{-2i\varphi}\\ \text{C.C.} & -\frac{1}{2}+\frac{4}{5}o_0\cos\theta-\frac{1}{6}a_0(3\cos^2\theta-1)+\frac{1}{30}e_0(5\cos^3\theta-3\cos\theta)\end{pmatrix}, \tag{25d}$$

4. Some Examples of Specific Optical Pumping Arrangements

We now turn to a discussion of some specific cases. We will be guided both by specific geometries for which data exists and by the desire to determine what geometries are required to effect complete determination of the scattering matrices.

4a. No Orientation, Alignment or Octopole Moment

While this situation is generally difficult to achieve experimentally, since light propagating uniaxially will usually induce at least some degree of alignment, it may be very nearly achieved under high density beam conditions. At sufficiently high density ($>10^{12}$ cm^{-3}), radiation trapping would tend to redistribute the radiation isotropically, generating the desired isotropic excitation. With $o_0=a_0=e_0=0$, the matrices in (25a–c) take on the very simple form

$$\boldsymbol{\sigma}_0=\tfrac{1}{3}\begin{pmatrix}1 & 0\\ 0 & 1\end{pmatrix}, \tag{26a}$$

$$\boldsymbol{\sigma}_z=\tfrac{1}{6}\begin{pmatrix}1 & 0\\ 0 & -1\end{pmatrix}, \tag{26b}$$

$$\boldsymbol{\sigma}_x=\boldsymbol{\sigma}_y=0. \tag{26c}$$

The interesting point here is that despite the fact that there is no orientation, alignment or octopole moment, there is still the possibility of a spin-dependent effect since $\boldsymbol{\sigma}_z\neq 0$. Using (24), the scattering intensity can now be written in terms of the elements of the scattering matrices **s** and **t** as

$$I=\frac{C}{12}\left\{3(t_{11}+t_{-1-1})+(s_{11}+s_{-1-1})+\frac{P_z}{2}[(t_{11}-t_{-1-1})-(s_{11}-s_{-1-1})]\right\}. \tag{27}$$

This intensity will be different depending on whether the incident electron spin is "up" ($P_z=+|P_z|$) or "down" ($P_z=-|P_z|$). One can thus construct a spin asymmetry from (27) as

$$A=\frac{1}{|P_z|}\frac{I(\uparrow)-I(\downarrow)}{I(\uparrow)+I(\downarrow)}, \tag{28}$$

where the arrows refer to spin "up" ($\uparrow$) or "down" ($\downarrow$). We get

$$A=\frac{1}{2}\frac{(t_{11}-t_{-1-1})-(s_{11}-s_{-1-1})}{3(t_{11}+t_{-1-1})+(s_{11}+s_{-1-1})}. \tag{29}$$

This spin asymmetry is what has been referred to as the "fine-structure" effect [10, 28, 29]. It arises solely because the atom has been prepared in a single

fine-structure state and because the singlet and triplet scattering intensities differ. It has nothing to do with spin-orbit coupling between the incident electron's spin and its angular momentum (which, after all is completely neglected in the present treatment), despite the fact that it occurs in a completely unpolarized atom.

4b. Circularly Polarized Pumping with Light Propagating Perpendicular to the Scattering Plane

Our next case is still relatively simple, and is of immediate interest because of the experiments recently conducted in this geometry (see Sect. 5). We have $\hat{\mathbf{z}}_{\text{photon}} = \hat{\mathbf{z}}_{\text{nat}}$, so the polar angles θ and φ are both equal to zero. Inserting these values into (25a–d) yields

$$\boldsymbol{\sigma}_0 = \tfrac{1}{3}\begin{pmatrix} 1+o_0+a_0/6 & 0 \\ 0 & 1-o_0+a_0/6 \end{pmatrix}, \tag{30a}$$

$$\boldsymbol{\sigma}_z = \tfrac{1}{3}\begin{pmatrix} \frac{1}{2}+\frac{4}{5}o_0+\frac{1}{3}a_0+\frac{1}{15}e_0 & 0 \\ 0 & -\frac{1}{2}+\frac{4}{5}o_0-\frac{1}{3}a_0+\frac{1}{15}e_0 \end{pmatrix}, \tag{30b}$$

$$\boldsymbol{\sigma}_x = \boldsymbol{\sigma}_y = 0. \tag{30c}$$

Now we can put in the stationary pumping values $o_0 = \pm 3/2$, $a_0 = 3$ and $e_0 = \pm 9/2$ given in (A8a–c), where the + and − signs correspond respectively to positive (right-handed, RHC) and negative (left-handed, LHC) helicity for the circularly polarized light propagating in the $+\hat{\mathbf{z}}_{\text{nat}}$ direction. This gives the simple result

$$\boldsymbol{\sigma}_0(\text{RHC}) = \begin{pmatrix} 1 & 0 \\ 0 & 0 \end{pmatrix}, \tag{31a}$$

$$\boldsymbol{\sigma}_z(\text{RHC}) = \begin{pmatrix} 1 & 0 \\ 0 & 0 \end{pmatrix}, \tag{31b}$$

$$\boldsymbol{\sigma}_0(\text{LHC}) = \begin{pmatrix} 0 & 0 \\ 0 & 1 \end{pmatrix}, \tag{31c}$$

$$\boldsymbol{\sigma}_z(\text{LHC}) = \begin{pmatrix} 0 & 0 \\ 0 & -1 \end{pmatrix}. \tag{31d}$$

Since $\boldsymbol{\sigma}_x = \boldsymbol{\sigma}_y = 0$ in this case, we see that P_z is the only component of the incident electron spin which can provide new information. Furthermore, since the off-diagonals of $\boldsymbol{\sigma}_0$ and $\boldsymbol{\sigma}_z$ are all zero, it is clear that nothing can be deduced from this experiment about the off-diagonals of the singlet and triplet matrices **s** and **t**.

Using (31a–d) in (24), we can write explicit expressions for the scattering intensity in terms of elements of the scattering matrices **s** and **t** as in the previous section:

$$I^R = \frac{C}{4}[(3+P_z)\,t_{11} + (1-P_z)\,s_{11}] \tag{32a}$$

$$I^L = \frac{C}{4}[(3-P_z)\,t_{-1-1} + (1+P_z)\,s_{-1-1}], \tag{32b}$$

where R and L refer respectively to plus and minus helicity of the light. If one does an experiment in which scattering is measured with electrons polarized either in the $+\hat{\mathbf{z}}_{\text{nat}}$ or $-\hat{\mathbf{z}}_{\text{nat}}$ direction, (32a–b) can be inverted to extract four experimental quantities which are proportional to the scattering matrix elements:

$$T_{11} = \frac{1}{2}\left[\left(\frac{1}{|P_z|}+1\right)I^{R\uparrow} - \left(\frac{1}{|P_z|}-1\right)I^{R\downarrow}\right] \propto t_{11}, \tag{33a}$$

$$T_{-1-1} = \frac{1}{2}\left[\left(\frac{1}{|P_z|}+1\right)I^{L\downarrow} - \left(\frac{1}{|P_z|}-1\right)I^{L\uparrow}\right] \propto t_{-1-1}, \tag{33b}$$

$$S_{11} = \frac{1}{2}\left[\left(\frac{3}{|P_z|}+1\right)I^{R\downarrow} - \left(\frac{3}{|P_z|}-1\right)I^{R\uparrow}\right] \propto s_{11}, \tag{33c}$$

$$S_{-1-1} = \frac{1}{2}\left[\left(\frac{3}{|P_z|}+1\right)I^{L\uparrow} - \left(\frac{3}{|P_z|}-1\right)I^{L\downarrow}\right] \propto s_{-1-1}. \tag{33d}$$

Here, we have added to the intensity I the superscripts $\uparrow$ to indicate scattering with electrons polarized in the $+\hat{\mathbf{z}}_{\text{nat}}$ direction ($P_z = +|P_z|$), and $\downarrow$ with electrons polarized in the $-\hat{\mathbf{z}}_{\text{nat}}$ direction ($P_z = -|P_z|$).

Because of difficulties associated with the absolute measurements necessary to extract the scattering matrix elements directly, it is worthwhile to define relative quantities which, together with one absolute measurement of the spin and orientation averaged differential cross section, are sufficient to completely determine the scattering matrices. Such relative quantities are more conveniently determined experimentally and also have more physical significance. As in the case of scattering with unpolarized electrons, we can extract the angular momentum transferred to the atom in the collision, but this time we generate two quantities (see (10a–b)), one for singlet, $L^s_\perp$, and one for triplet, $L^t_\perp$. They are given by

$$L^t_\perp = \frac{T_{11}-T_{-1-1}}{T_{11}+T_{-1-1}} = \frac{t_{11}-t_{-1-1}}{t_{11}+t_{-1-1}}, \tag{34a}$$

$$L^s_\perp = \frac{S_{11}-S_{-1-1}}{S_{11}+S_{-1-1}} = \frac{s_{11}-s_{-1-1}}{s_{11}+s_{-1-1}}. \tag{34b}$$

The ratio, r, between singlet and triplet contributions to the scattering intensity (see (12)) is given by

$$r=\frac{(T_{11}+T_{-1-1})}{(S_{11}+S_{-1-1})}=\frac{(t_{11}+t_{-1-1})}{(s_{11}+s_{-1-1})}. \tag{35}$$

These three parameters contain all the information one can obtain from the relative measurements of the four quantities $I^{R\uparrow}$, $I^{R\downarrow}$, $I^{L\uparrow}$, and $I^{L\downarrow}$.

4c. *Linearly Polarized Pumping with Light Propagating Perpendicular to the Scattering Plane*

This case is of interest first, because experiments have been conducted in this geometry [11], and second because it is an experimentally accessible example of a spin-dependence in the scattering of polarized electrons from an atom whose electron is not spin-polarized. For this example, $\hat{\mathbf{z}}_{\text{photon}}$ lies in the scattering plane, so the polar angle θ takes the value $\frac{\pi}{2}$. The azimuthal angle φ is the angle between $\hat{\mathbf{x}}_{\text{nat}}$ and the electric vector of the light, measured in a positive sense about $\hat{\mathbf{z}}_{\text{nat}}$. The only optical pumping parameter is a_0, which has the value -2. Using (25a–d), we obtain

$$\boldsymbol{\sigma}_0=\frac{1}{6}\begin{pmatrix} 7/3 & -e^{-2i\varphi} \\ -e^{2i\varphi} & 7/3 \end{pmatrix}, \tag{36a}$$

$$\boldsymbol{\sigma}_z=\frac{5}{18}\begin{pmatrix} 1 & 0 \\ 0 & -1 \end{pmatrix}, \tag{36b}$$

$$\boldsymbol{\sigma}_x=\boldsymbol{\sigma}_y=0. \tag{36c}$$

Comparing these matrices to those in Sect. 4a, where the situation with no orientation, alignment or octopole moment was considered, one sees a remarkable similarity, especially in $\boldsymbol{\sigma}_z$. This matrix has exactly the same form as before, the only difference being that it is multiplied by a different constant. Thus we should expect the spin-dependent part of the scattering intensity to have much the same behavior. The matrix $\boldsymbol{\sigma}_0$ has diagonal elements similar to those in the previous case, but it also has nonzero off-diagonal elements. These off-diagonal elements indicate that now the scattering intensity (see (8, 10a–b)) is sensitive to the off-diagonal element $-P_{\text{lin}}e^{-2i\gamma}$ in the matrix sum $(3\mathbf{t}+\mathbf{s})$. Hence one might be able to probe these by varying the angle φ. We note, however, that since the off-diagonals occur in $\boldsymbol{\sigma}_0$ and not in $\boldsymbol{\sigma}_z$, one obtains no new information on the scattering matrix off-diagonals by spin-polarizing the incident electrons. The φ-dependence in the intensity is exactly the same as is observed in an unpolarized experiment.

Let us write the intensity down in explicit form as

$$I=\frac{C}{72}Q_0\{7-3[(3t_{1-1}+s_{1-1})e^{2i\varphi}+\text{C.C.}] +5P_z(t_{11}-t_{-1-1}+t_{11}-t_{-1-1})\}, \tag{37}$$

where to obtain this result we have used (36a–b) in (24) and the normalization of (11). The expression for the intensity (37) can be rewritten in terms of previously determined experimental quantities in the form

$$I=\frac{C}{72}Q_0\{7+3P_{\text{lin}}\cos 2(\varphi-\gamma)+5P_z\,\Delta L_\perp\}, \tag{38}$$

where $\Delta L_\perp$ is a "weighted difference" between the triplet and singlet contributions to $L_\perp$. In terms of the three relative quantities measured in the circular polarization experiment described in Sect. 4b. $\Delta L_\perp$ can be expressed as

$$\Delta L_\perp=\frac{(t_{11}-t_{-1-1})-(s_{11}-s_{-1-1})}{Q_0}=\frac{1}{3r+1}(rL^t_\perp-L^s_\perp) \tag{39}$$

where (11.34a–b) have been used.

In order to make the connection with the experiment of reference [11], we construct, as in (28), a spin asymmetry given by

$$A=\frac{5\Delta L_\perp}{7+3P_{\text{lin}}\cos 2(\varphi-\gamma)}. \tag{40}$$

Thus we see that although this experiment is an interesting example of the "fine-structure effect" [10, 28, 29], it provides no new information about the matrices $\mathbf{t}$ and $\mathbf{s}$ that could not be obtained from experiments with unpolarized electrons combined with polarized-electron experiments with circularly polarized optical pumping. Nevertheless, taking P_{lin}, γ and $\Delta L_\perp$ from previous measurements, one can use (40) to predict a spin asymmetry with well-defined φ-dependence. This can then be measured to verify the underlying assumptions of the approach outlined in this paper. More discussion of this will be presented in Sect. 5.

4d. *Circularly Polarized Pumping with Arbitrary Angle of Incidence*

In the previous sections we have seen that it is possible to measure $L^t_\perp$, $L^s_\perp$ and r with polarized electrons and circularly polarized pumping, and P_{lin} and γ with

unpolarized electrons and linearly polarized pumping. However, complete characterization of the matrices **t** and **s** requires more information, namely separate determinations of P_{lin}^t, P_{lin}^s, γ^t and γ^s. Clearly, in order to achieve this one must find an optical pumping scheme in which $\boldsymbol{\sigma}_z$ (or $\boldsymbol{\sigma}_x$ or $\boldsymbol{\sigma}_y$) has off-diagonal elements. Then the scattering intensity will contain a term proportional to $(t_{1-1}-s_{1-1})$, which, in combination with the information on $(3t_{1-1}+s_{1-1})$ obtained with unpolarized electrons, can be used to extract the necessary information. An angular variable in the off-diagonal of $\boldsymbol{\sigma}_z$ will also be useful, as this makes possible the extraction of the phase angles γ^t and γ^s.

Using again electron spin polarization perpendicular to the scattering plane, exploiting $\boldsymbol{\sigma}_z$, we see from (25d) that the first important criterion is that we create an atom with an octopole moment e_0.[3] If we restrict ourselves to pure polarization, either circular or linear, it is clear that we must choose circular polarization, since linear polarization produces only an alignment a_0.

Next we must ensure that the choice of photon frame does not make the off-diagonals in $\boldsymbol{\sigma}_z$ vanish as it did in Sect. 4b. For example, one might let $\theta=54.74°$, the "magic angle" of photoelectron spectroscopy, which maximizes the product $\sin^2\theta\cos\theta$, creating the largest possible off-diagonal element. Then, using the stationary optical pumping values for o_0, a_0, and e_0, $\boldsymbol{\sigma}_0$ becomes

$$\boldsymbol{\sigma}_0=\tfrac{1}{6}\begin{pmatrix}2\pm\sqrt{3} & \mathrm{e}^{-2i\varphi}\\ \mathrm{e}^{2i\varphi} & 2\mp\sqrt{3}\end{pmatrix}. \tag{41}$$

while the matrix $\boldsymbol{\sigma}_z$ evaluates to

$$\boldsymbol{\sigma}_z=\frac{1}{6\sqrt{3}}\begin{pmatrix}\sqrt{3}\pm 2 & \pm\mathrm{e}^{-2i\varphi}\\ \pm\mathrm{e}^{2i\varphi} & -\sqrt{3}\pm 2\end{pmatrix} \tag{42}$$

(in each dual sign, the upper sign is for RHC light and the lower sign is for LHC light). The matrices $\boldsymbol{\sigma}_x$ and $\boldsymbol{\sigma}_y$ are no longer zero, but they can be ignored if we restrict ourselves to incident electrons polarized along $\hat{\mathbf{z}}_{\text{nat}}$. As in the previous section, we can write down the intensity using (24). From this, we can construct a spin asymmetry, as defined in (28). After some algebra, one obtains

$$A=\frac{1}{\sqrt{3}}\,\frac{\sqrt{3}\,\Delta L_\perp\pm 2\dfrac{r-1}{3r+1}\mp D_{\text{lin}}\cos 2(\varphi-\delta)}{2-P_{\text{lin}}\cos 2(\varphi-\gamma)\pm\sqrt{3}\,\Delta L_\perp}. \tag{43}$$

[3] Note that terms which contain octopole moments are typical for the optical pumping approach to the scattering process. In contrast, electron-photon coincidence experiments for the inverse process would only provide multipole moments up to rank 2 [15] in the $\boldsymbol{\sigma}_0$, $\boldsymbol{\sigma}_x$, $\boldsymbol{\sigma}_y$, and $\boldsymbol{\sigma}_z$ matrices and the presently discussed setup would not provide any new information

Here we have introduced the new quantities D_{lin} and 2δ as the magnitude and phase of the normalized off-diagonal element $(t_{1-1}-s_{1-1})/Q_0$, in analogy to P_{lin} and 2γ:

$$-\frac{1}{2}D_{\text{lin}}\,\mathrm{e}^{-2i\delta}=\frac{(t_{1-1}-s_{1-1})}{Q_0}. \tag{44}$$

Presuming that practical considerations do not interfere, this, then, is one possible approach towards measurement of all possible information about the matrices **t** and **s**. One might consider an experiment in which the spin asymmetry is measured while φ is varied. Then, since all parameters in (43) are available from other measurements except D_{lin} and 2δ, these two could be extracted. Knowing these as well as P_{lin} and 2γ, which give the magnitude and phase of the sum $(3t_{1-1}+s_{1-1})$, then allows complete determination of the magnitude and phase of t_{1-1} and s_{1-1} separately (see Sect. 4e).

An alternative and sometimes more practical approach would be to use a spin polarization vector $\mathbf{P}_e=(P_x, P_y, 0)$ in the $\hat{\mathbf{x}}_{\text{nat}}-\hat{\mathbf{y}}_{\text{nat}}$ scattering plane and circularly polarized light propagating parallel to $\mathbf{P}_e$. To obtain that geometry experimentally from the setup discussed in Sect. 4b, one might, for example, simply rotate the electron detector plane through 90°, leaving the incident electron beam direction, spin polarization and direction of the light propagation unchanged. Then the matrices $\boldsymbol{\sigma}_x$ and $\boldsymbol{\sigma}_y$ become important because their off-diagonal elements contain both octopole moments *and* orientation.[4] With $\cos\theta=0$, $P_x=\pm|\mathbf{P}_e|\cos\varphi$, and $P_y=\pm|\mathbf{P}_e|\sin\varphi$, we note, without going into detail, that rather simple expressions for the spin asymmetry arise. They contain again D_{lin} and δ. A measurement with (RHC) ad (LHC) light would allow us to determine these quantities.

The approaches suggested here are by no means the only possibilities to obtain information about the off diagonal elements. As can be seen from (25d), there are many optical pumping configurations which lead to a nonzero off-diagonal in $\boldsymbol{\sigma}_z$, though some may experimentally be more accessible than others. In addition, if one is willing to consider ellipitically polarized light, then the possibilities become even more varied. However, one is forced to use a more complicated expression for $\boldsymbol{\sigma}_z$, since (25d) is no longer valid. If the optical pumping can be properly controlled and completely analyzed, this may indeed be a more appropriate way to approach the problem, but a very careful analysis would have to be carried out before such an experiment were attempted.

[4] Thus, this approach would be applicable to electron-photon coincidence experiments as well

4e. Relations Between the Matrix Elements

Assume we have determined by studies with circularly polarized light and spin polarization the quantities $L^t_\perp$ and $L^s_\perp$ and the cross section ratio r as described in the preceding section, and have determined by some means D_{lin} and δ as well. Assume also that P_{lin} and γ are known from studies using linearly polarized excitation, but without spin polarization. It is then possible to determine, in the same normalization, all matrix elements of the triplet and singlet scattering matrices **s** and **t**. From the definitions (10–12, 44) we obtain for the four real diagonal elements

$$\frac{t_{11}}{Q_0} = \frac{1}{2}\frac{r}{(3r+1)}(1+L^t_\perp), \tag{45a}$$

$$\frac{t_{-1-1}}{Q_0} = \frac{1}{2}\frac{r}{(3r+1)}(1-L^t_\perp), \tag{45b}$$

$$\frac{s_{11}}{Q_0} = \frac{1}{2}\frac{1}{(3r+1)}(1+L^s_\perp), \tag{45c}$$

$$\frac{s_{-1-1}}{Q_0} = \frac{1}{2}\frac{1}{(3r+1)}(1-L^s_\perp) \tag{45d}$$

and for the complex off-diagonal elements we have

$$\frac{t_{1-1}}{Q_0} = -\tfrac{1}{2}P^t_{\text{lin}}\,e^{-2i\gamma^t} = -\tfrac{1}{8}(P_{\text{lin}}\,e^{-2i\gamma} + D_{\text{lin}}\,e^{-2i\delta}), \tag{46a}$$

$$\frac{s_{1-1}}{Q_0} = -\tfrac{1}{2}P^s_{\text{lin}}\,e^{-2i\gamma^t} = -\tfrac{1}{8}(P_{\text{lin}}\,e^{-2i\gamma} - 3D_{\text{lin}}\,e^{-2i\delta}). \tag{46b}$$

Up to now we have discussed the evaluation procedure as if all these matrix elements were completely independent. In that way these relations may be used even for more complex cases than the $np \leftrightarrow n's$ transition which is our primary concern at present.[5] For an $np \leftrightarrow n's$ transition the situation simplifies in as far as there are only four complex amplitudes, one set for triplet and one set for singlet scattering, f^t_M and f^s_M.

The relative phases of these four amplitudes are more clearly seen if the amplitudes are expressed as $|f^t_{\pm1}|\exp(i\phi^t_{\pm1})$ and $|f^s_{\pm1}|\exp(i\phi^s_{\pm1})$. As the overall phase is arbitrary and unobservable, we factor out and ignore a common average phase of $\frac{1}{4}(\phi^t_1+\phi^t_{-1}+\phi^s_1+\phi^s_{-1})$ from each amplitude. One is left with three relative phases, which we take to be first, a relative phase between singlet and triplet scattering, defined as

$$2\delta^{st} = \tfrac{1}{2}(\phi^s_1+\phi^s_{-1}) - \tfrac{1}{2}(\phi^t_1+\phi^t_{-1}) \tag{47a}$$

and next, two relative phases between $+1$ and -1 amplitudes, defined as

$$2\delta^s = \phi^s_1 - \phi^s_{-1}, \tag{47b}$$

$$2\delta^t = \phi^t_1 - \phi^t_{-1}. \tag{47c}$$

We note that since the singlet-triplet relative phase, δ^{st}, will appear in none of the scattering matrices here derived, it cannot be determined in this type of experiment. Spin analysis of the electron (and/or atom) would additionally be required to study this relative phase.

With these definitions, we write the four amplitudes as

$$f^s_{\pm1} = |f^s_{\pm1}|\,e^{i(\delta^{st}\pm\delta^s)}, \tag{48a}$$

$$f^t_{\pm1} = |f^t_{\pm1}|\,e^{i(-\delta^{st}\pm\delta^t)}, \tag{48b}$$

and the matrix elements of **t** and **s** as

$$t_{11} = |f^t_1|^2, \tag{49a}$$

$$t_{-1-1} = |f^t_{-1}|^2, \tag{49b}$$

$$s_{11} = |f^s_1|^2, \tag{49c}$$

$$s_{-1-1} = |f^s_{-1}|^2, \tag{49d}$$

and

$$t_{1-1} = f^{t*}_1 f^t_{-1} = |f^t_1||f^t_{-1}|\,e^{-2i\delta^t} = -|f^t_1||f^t_{-1}|\,e^{-2i\gamma^t}, \tag{50a}$$

$$s_{1-1} = f^{s*}_1 f^s_{-1} = |f^s_1||f^s_{-1}|\,e^{-2i\delta^s} = -|f^s_1||f^s_{-1}|\,e^{-2i\gamma^s}. \tag{50b}$$

We note that the alignment angles, γ^s and γ^t, of the collisionally excited atom are very closely related to relative phases between the $+1$ and -1 scattering amplitudes. In fact, the phase differences, δ^s and δ^t merely define the alignment of the minor axis, rather than the major axis, of the collisionally excited charge cloud. For consistency with previous work, we will henceforth use the alignment angles for the major axes, γ^s and γ^t, to characterize the phase of the off-diagonal elements.

We see from (47a–b) that the off-diagonal elements of **t** and **s** are already known in magnitude if the diagonal terms are available. Thus we are left with the task to determine the phase angles γ^t and γ^s (as defined in (10a–b, 50a–b)), while the linear polarization parameters for singlet and triplet scattering may be derived from the diagonal matrix elements, i.e., from studies with spin polarization and circularly polarized light (see (45a–d)):

$$P^t_{\text{lin}} = 2\frac{3r+1}{r}\frac{\sqrt{t_{11}\,t_{-1-1}}}{Q_0} = \sqrt{1-(L^t_\perp)^2}, \tag{51a}$$

[5] Note, however, that for transitions other than $p \leftrightarrow s$, the assumption $\rho_{00}=0$ has dropped so that the analysis becomes somewhat more involved, even though straightforward

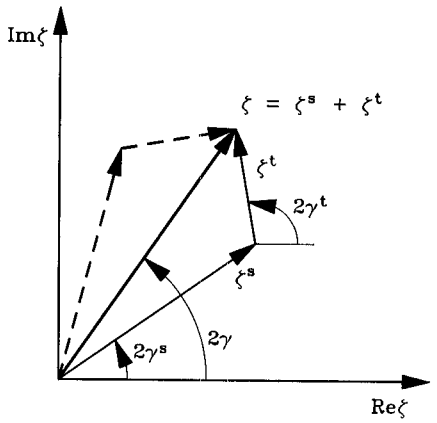

Fig. 1. Graphic representation of (52) in the complex plane. The two terms on the right-hand side of the equation are represented by the vectors ζ^s and ζ^t, and the left-hand side is represented by the vector ζ. Note that if $|\zeta|$, γ, $|\zeta^s|$ and $|\zeta^t|$ are known, there are two ways in which the vectors ζ^s and ζ^t can add to yield ζ, as illustrated by the solid and dashed vectors. Thus two sets of values for γ^s and γ^t are possible, given the information at hand

$$P_{\text{lin}}^s = 2(3r+1)\frac{\sqrt{S_{11}\,S_{-1-1}}}{Q_0} = \sqrt{1-(L_\perp^s)^2} \tag{51b}$$

where we ave used (10a–b, 11).

If we now recall the definition of P_{lin} and γ for the unpolarized case from (8), we may use (51a–b) to rewrite the off-diagonal element of the spin unpolarized density matrix and obtain

$$P_{\text{lin}}\,e^{-2i\gamma} = \frac{1}{3r+1}(3rP_{\text{lin}}^t\,e^{-2i\gamma^t} + P_{\text{lin}}^s\,e^{-2i\gamma^s}). \tag{52}$$

Thus we have already a (complex) equation which relates the known parameters P_{lin}, γ, P_{lin}^t, P_{lin}^s, and r, to the remaining unknown phase angles γ^t and γ^s so that one may hope to avoid the somewhat tedious determination of D_{lin} and δ in the present case.

This is, however, only partially correct. Figure 1 illustrates the addition of the two right hand terms of (52), abbreviated as ζ^t and ζ^s, to give $\zeta = P_{\text{lin}}\,e^{-2i\gamma}$. As one can see, two solutions are possible for γ^s and γ^t. Even with this ambiguity it may sometimes be very worthwhile to evaluate the two alternative sets of γ^t and γ^s for comparison with theory. A final decision of which set is correct requires either the determination of δ, as discussed in the previous section, or some other experiment to distinguish between the alternate solutions for γ^s and γ^t.

It should be noted that the situation discussed here is quite similar to that encountered in a $s \to d$ heavy particle impact excitation without spin analysis as discussed by Andersen et al. [30, 31].

5. Experimental Results

We now apply the results of the preceding sections to a reevaluation of the experimental data of McClelland et al. [11, 12], who presented spin asymmetries for the collisional deexcitation process defined in (1). We give here only a brief summary of the relevant experimental details.

A beam of spin-polarized electrons, produced in a GaAs negative-electron-affinity photoemission source [32], intersected a beam of sodium atoms prepared in a well defined excited state by laser optical pumping. The polarization of the electron beam was typically $|P_z| = 0.26 \pm 0.02$ [11, 12]. The intersection of the two beams defined the center of a horizontal scattering plane, in which rotated a channel electron multiplier incorporating a retarding field energy analyzer. This detector rejected all elastically or inelastically scattered electrons, while allowing detection of the 2.1 eV more energetic superelastically scattered electrons. The optical pumping laser, locked to the $3^2S_{1/2}(F=2) \to 3^2P_{3/2}(F=3)$ transition in sodium, was either linearly or circularly polarized to achieve the desired state preparation of the excited sodium atoms.

5a. *Circularly Polarized Excitation*

Figure 2 shows a schematic of the scattering geometry from [12], displaying the direction of the incident electron beam ($\mathbf{k}_i$), the scattered electrons ($\mathbf{k}_f$), and the electron spin polarization $\mathbf{P}_e$ which is parallel to the $\hat{\mathbf{z}}$-axis in the natural frame, indicated by $\hat{\mathbf{x}}_{\text{nat}}$, $\hat{\mathbf{y}}_{\text{nat}}$, and $\hat{\mathbf{z}}_{\text{nat}}$. Notice that the optical pumping light, incident from above the scattering plane, propagates in

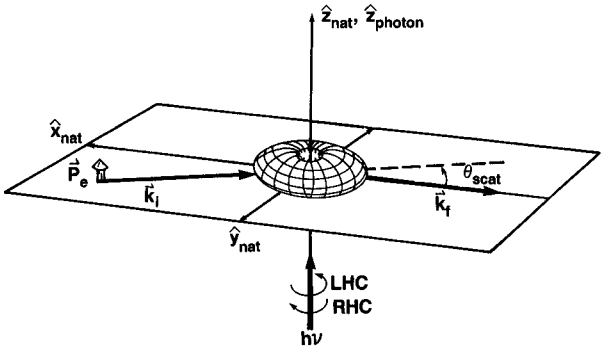

Fig. 2. Schematic of the scattering geometry for circularly polarized optical pumping, showing the orientations of the natural and photon frames. Electrons of polarization $\mathbf{P}_e = P_e\,\hat{\mathbf{z}}_{\text{nat}}$ are incident with momentum $\mathbf{k}_i$ and scatter into an angle θ_{scat} with momentum $\mathbf{k}_f$. The laser, with left-handed (LHC) or right-handed (RHC) circular polarization, is incident along the $\hat{\mathbf{z}}_{\text{nat}}$ direction. The photon frame and the natural frame coincide in this case

the $-\hat{\mathbf{z}}_{\text{nat}}$ direction. We thus take the photon frame to be such that $\hat{\mathbf{z}}_{\text{photon}} = -\hat{\mathbf{z}}_{\text{nat}}$.

The typical measurement protocol consisted of modulating the spin of the incident electron beam, counting the scattered electrons for each spin direction separately with two gated scalers. For measurements with circularly polarized pumping light, the helicity of the optical pumping laser was periodically reversed so that, in total, four count rates were recorded, one for each of the possible combinations of electron and atom spin directions. A background signal was recorded with the laser blocked. Series of such measurements were undertaken as a function of scattering angle at two fixed incident energies of 2.0 and 9.26 eV, and as a function of incident energy at a scattering angle of 30°.

The four scattering signals are used to calculate the three relative quantities $L^t_\perp$, $L^s_\perp$, and r, as discussed in Sect. 4b. One first calculates, according to (33a–d), the intermediate quantities T_{11}, T_{-1-1}, S_{11}, and S_{-1-1}, which are the signals one would expect if one could prepare pure singlet and triplet initial states. From these, one calculates the relative quantities according to (34a–b, 35). The results are shown in Figs. 3 through 5. In all figures, the solid points are the experimental results with error estimates of one standard deviation from counting statistics.

For an incident energy of 2.0 eV, corresponding to an energy of 4.1 eV for the reverse process, i.e. inelastic scattering from the sodium ground state, these quantities were measured as a function of scattering angle in the angular range from 10° to 40°, with the results shown in Fig. 3. As seen in Fig. 3a, the angular momentum is more effectively transferred through the triplet than through the singlet scattering channel. In either case, the angular momentum transfer peaks at about 35°, perhaps slightly earlier for singlet than for triplet. The data for the triplet channel are consistent with complete angular momentum transfer of $L_\perp = 1$ at a scattering angle of 35°. Thus excitation of Na(3S) into the 3P-state by pure triplet scattering would leave the excited atom in a fully circular state ($M_L = 1$). In this range of scattering angles, the ratio of triplet to singlet scattering, shown in Fig. 3b, is roughly constant with singlet about 30% larger. The 4-state close-coupling results of Moores and Norcross [20], at 4.0 eV, are included, for comparison, as the solid solid lines in Fig. 3.[6] As expected,

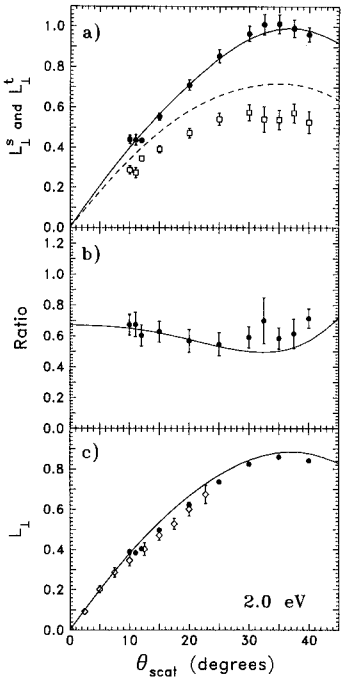

Fig. 3a–c. Angular dependence of parameters discussed in the text at an incident energy of 2.0 eV (superelastic), corresponding to an inelastic energy of 4.1 eV. Experimental results are a reevaluation of data from McClelland et al. [12] unless otherwise stated. Theory is the four-state close-coupling calculation of [20] at 4.0 eV. **a** Triplet angular momentum transfer $L^t_\perp$ (● experiment; ——— theory) and singlet angular momentum transfer $L^s_\perp$ (□ experiment; – – – – theory). **b** Triplet-singlet ratio $r = Q^t_o/Q^s_o$ (● experiment; ——— theory). **c** Angular momentum transferred by unpolarized electrons $L_\perp$ (● experiment; ◇ experiment of Hermann and Hertel [13] at 3.0 eV; ——— theory). Error bars are one standard deviation derived from counting statistics

at this incident energy, the close-coupling calculations agree quite well with the experimental results. It is interesting to note that while the agreement for the cross section ratio and for the triplet angular momentum transfer is quite good, the agreement is somewhat less satisfying for the angular momentum transferred via the singlet channel.

In Fig. 3c, these spin-polarized measurements have been averaged to give the angular momentum transferred in collisions by unpolarized electrons in order to compare with the earlier measurements of Hermann et al. [13]. Despite the difference in incident energy (3 eV vs. 2 eV), the agreement is quite good.

At an incident energy of 9.26 eV, corresponding to an energy of 11.36 eV for inelastic scattering, the data, shown in Fig. 4, show somewhat different behavior. Figure 4a indicates that the triplet angular momentum transfer peaks at smaller scattering angle and has a smaller peak value than at lower energy. Though the data for the singlet $L_\perp$ have more scatter,

[6] Note that the scattering amplitudes have been calculated with respect to the standard collision frame. For our comparison they are transformed, as discussed in Sect. 3a, into the natural frame [17, 18] by

$$f^{\text{nat}}_{\pm 1} = \mp \frac{1}{\sqrt{2}} f^{\text{col}}_0 - i f^{\text{col}}_1$$

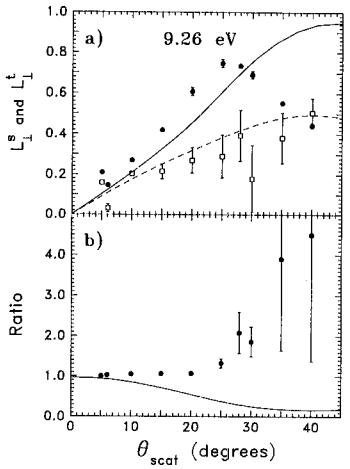

Fig. 4a and b. Angular dependence of parameters discussed in the text at an incident energy of 9.26 eV (superelastic), corresponding to an inelastic energy of 11.36 eV. Experimental results are a reevaluation of data from McClelland et al. [12]. Theory is the distorted-wave polarized-orbital calculation of [21] at 12.1 eV. **a** Triplet angular momentum transfer $L^t_\perp$ (● experiment; ——— theory), and singlet angular momentum transfer $L^s_\perp$ (□ experiment; – – – theory). **b** Triplet-singlet ratio $r = Q^t_o/Q^s_o$ (● experiment; ——— theory). Error bars are one standard deviation from counting statistics

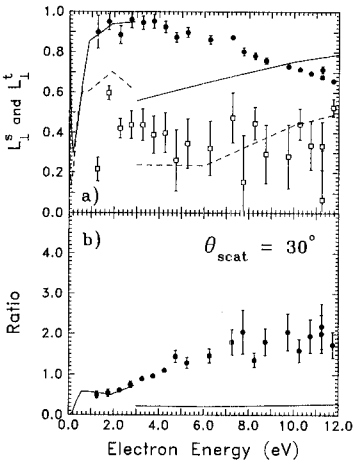

Fig. 5a and b. Energy dependence of parameters discussed in the text at a scattering angle $\theta_{scat} = 30°$. Energy is superelastic incident energy, so 2.1 eV must be added for comparison with inelastic results. Experimental results are a reevaluation of data from McClelland et al. [12]. Theory is four-state close-coupling of [20] up to 2.9 eV, and distorted-wave polarized-orbital of [21] thereafter. **a** Triplet angular momentum transfer $L^t_\perp$ (● experiment; ——— theory) and singlet angular momentum transfer $L^s_\perp$ (□ experiment; – – – theory). **b** Triplet-singlet ratio $r = Q^t_o/Q^s_o$ (● experiment; ——— theory). Error bars are one standard deviation from counting statistics

there is indication that the transfer efficiency may peak at an angle larger than 40°. In Fig. 4b, we see that the relative strengths of singlet and triplet scattering are about equal at small angles, up to about 25°, with triplet dominating at larger angles. At this energy, the experimental data are compared with the results of a distorted-wave polarized-orbital (DWPO) calculation at 12.1 eV by Kennedy et al. [21], included in Fig. 4 as the dashed lines. While this theory agrees reasonably with $L^s_\perp$ and with $L^t_\perp$ small angles, it does so at the expense of completely missing the overall trend toward triplet dominant scattering as the scattering angle increases.

At one scattering angle, 30°, experimental data are available as a function of incident energy from 1.3 eV to 12 eV, with the results shown in Fig. 5. Again, angular momentum is tranferred more efficiently via the triplet than the singlet scattering. The triplet $L_\perp$ has a broad maximum around 3 eV, then decreases slowly with increasing energy. The singlet $L_\perp$ appears roughly independent of energy in this energy range. The triplet to singlet cross section ratio shows roughly a monotonic increase with incident energy. Also shown in Fig. 5 are results from both close-coupling [20] (solid lines) and DWPO [21] (broken lines) at a few specific energies marked by the crosses. The close coupling results are in quite good agreement for $L^t_\perp$ and for the triplet to singlet ratio, with significantly larger discrepancy for $L^s_\perp$. The apparent tendency of the close coupling results to show poorer agreement for the singlet angular momentum is not understood at present. As for the 9.26 eV case, the DWPO calculation shows reasonable agreement strengths of singlet and triplet scattering as well as the overall energy dependence for $L^t_\perp$, which is the dominating term.

A different way of thinking about these results is in terms of direct and exchange scattering, the corresponding amplitudes being the difference and sum of singlet and triplet scattering amplitudes. Since the presently discussed experiment cannot determine the relative phase between singlet and triplet scattering amplitudes, a quantitative evaluation in terms of direct and exchange scattering is not possible. One may, however, note that exchange could only be small when singlet and triplet scattering amplitudes are of the same magnitude. Thus our finding of a large cross section ratio $Q^t_0/Q^s_0 > 1$ indicates a substantial exchange contribution to the scattering. This appears surprising at an energy about twice the ionization threshold and at not too large scattering angles. The DWPO calculations also indicate a large exchange contribution ($Q^t_0/Q^s_0 \ll 1$), however with a completely wrong phase factor.

5b. Linearly Polarized Light

As discussed in Sect. 4c, no new information can be obtained from studies with linearly polarized excita-

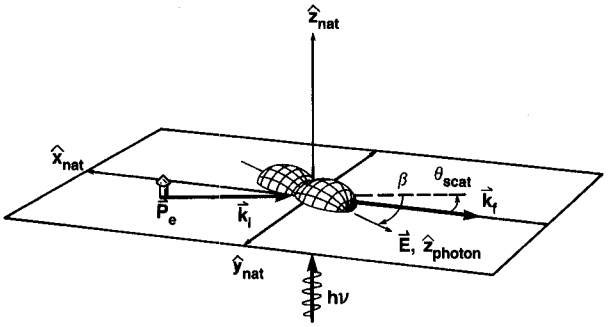

Fig. 6. Schematic of the scattering geometry for linearly polarized optical pumping, showing the orientations of the natural and photon frames. Electrons of polarization $\mathbf{P}_e = P_e \hat{\mathbf{z}}_{nat}$ are incident with momentum $\mathbf{k}_i$ and scatter into an angle θ_{scat} with momentum $\mathbf{k}_f$. The laser is incident along $\hat{\mathbf{z}}_{nat}$. The electric vector $\mathbf{E}$ of the laser light, which determines the direction of $\hat{\mathbf{z}}_{photon}$, makes an angle β with respect to the incident electron direction

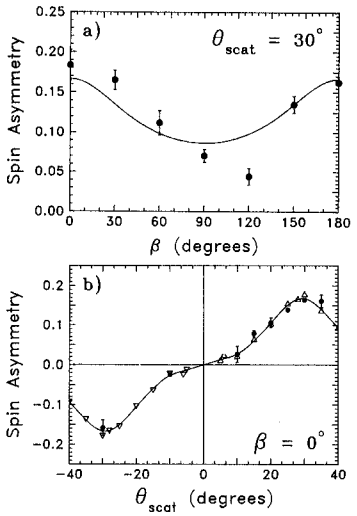

Fig. 7a and b. Spin asymmetry for superelastic scattering with linearly polarized optical pumping. The incident energy is 10.0 eV. **a** Asymmetry at a scattering angle $\theta_{scat} = 30°$ vs. the angle β which the electric vector of the laser light makes with respect to the incident electron direction (see Fig. 6) (● experimental data from [11], —— theory as discussed in Sect. 5b). **b** Asymmetry vs. scattering angle with $\beta = 0°$. (● experimental data from [11], △ and ▽ experimental data from [12], reprocessed as discussed in Sect. 5b)

tion of the target atom. However, since measurements with linearly polarized light have been reported and showed an interesting structure, it is useful to analyze these data in terms of what has been obtained with circularly polarized light [12], combined with the spin unpolarized results [13]. This will provide an interesting consistency check, illuminating what has been discussed in Sect. 4e. Also, proper definition of the coordinate frames becomes crucial at this point and our discussion will illustrate some of the subtleties which enter in the more general type of geometry discussed in Sect. 4d.

Figure 6 shows the geometry as defined by the primary beam ($\mathbf{k}_i$), scattered electrons ($\mathbf{k}_f$) and the electric vector $\mathbf{E}$ of the laser, which defines the $\hat{\mathbf{z}}_{photon}$ axis. Notice that the experimental polarization angle, β, of the electric vector $\mathbf{E}$ is measured with respect to the laboratory fixed axis $\mathbf{k}_i$. Thus, the azimuthal angle of $\hat{\mathbf{z}}_{photon}$ with respect to the natural frame, as defined in Fig. 8 is given by $\varphi = \pi + \theta_{scat} - \beta$. Measurements were also reported in [11] at "negative" scattering angles. In our present description, however, where $\hat{\mathbf{x}}_{nat}$ and $\hat{\mathbf{y}}_{nat}$ are always defined with respect to $\mathbf{k}_i$ and $\mathbf{k}_f$, scattering angles are always "positive". We account for the "negative" angles by writing $\varphi = |\theta_{scat}| \mp \beta$, where "$\mp$" refers to the "positive" and "negative" scattering angles of [11]. Equation (40) for the spin asymmetry then becomes

$$A = \pm \frac{5 \Delta L_\perp}{7 + 3 P_{lin} \cos 2(|\theta_{scat}| \mp \beta - \gamma)}. \tag{53}$$

The overall "$\mp$" sign accounts for the fact that, in the experiment, the spin polarization $\mathbf{P}_e$ is always defined with respect to the same laboratory fixed frame, while the $\hat{\mathbf{z}}_{nat}$ axis reverses direction for the "negative" angles.

Two types of measurements of the spin asymmetry, A, were performed. First, at a fixed scattering angle of $\theta_{scat} = 30°$, A was measured as a function of β. Next, at a fixed linear polarizer angle of $\beta = 0$, A was measured as a function of θ_{scat}. Figures 7a and 7b reproduce the experimental results of [11], adopting our present notations. As a consistency check, we also show analogous quantities derived from quantities measured with linearly polarized light without spin analysis [13] and from the previously discussed results circular polarization studies with spin analysis [12].

This comparison between the different types of experiments was made using the following procedure. First, notice that at a given scattering angle θ_{scat} one may obtain an estimate for $\Delta L_\perp$ from the spin asymmetry A averaged over β:

$$\Delta L_\perp \simeq \langle A \rangle_\beta \tfrac{7}{5}. \tag{54}$$

From Fig. 7a one obtains $\Delta L_\perp = 0.164$ at $\theta_{scat} = 30°$, while from the circularly polarized studies we find $r = 2.2$, $L^s_\perp = 0.35$, and $L^t_\perp = 0.70$, as taken from Figs. 4a and 4b. With (39), this gives $\Delta L_\perp = 0.156$ which indicate quite reasonable consistency between the two measurements, well within the limits of error.

Also from the circularly polarized data we can derive $P^t_{lin} = 0.71$ and $P^s_{lin} = 0.94$. With this and (52) we get an upper bound to for P_{lin} of 0.74 by assuming

equality of the phases γ^t and γ^s. P_{lin} as well as γ have been determined previously [13], unfortunately only up to $\theta_{\text{scat}}=20°$. An "educated guess" (based on the results electron scattering from H and He [1]) allows us to extrapolate these data to $P_{\text{lin}}(30°)\simeq 0.75\pm 0.1$ and $\gamma(30°)\simeq -60°\pm 10°$. For consistency we thus use the values $\Delta L_\perp=0.156$ and $P_{\text{lin}}=0.74$ derived from the circular polarization data together with $\gamma=60°$ to evaluate (53) as a function of β. The result is the solid line in Fig. 7a, which shows reasonable consistancy of all the data.

In a similar manner we have reanalyzed the circular polarization data [12] at different scattering angles (using "educated guesses" for γ where measurements are not available) to derive linearly polarized asymmetries, shown as the open symbols in Fig. 7b. Again we have used upper bounds for P_{lin} derived from the circular data, which agree well with previously measured values for P_{lin} [13] where available (e.g., the upper bound is 0.96 and 0.92 for $\theta_{\text{scat}}=10°$ and 20°, while the earlier values reported for P_{lin} are 0.89 and 0.86 ± 0.1 respectively [13]). Since the spin asymmetry is antisymmetric in scattering angle for $\beta=0°$, the reanalyzed data of [12], represented by the symbols $\triangle$, have been folded over to "negative angles" to give the points represented by the symbols $\triangledown$. As seen in Fig. 7b the linear polarization data [11] show a nice consistency with the recalculated data from the circularly polarized experiment [12].

6. Conclusions

To summarize, we have extended the density matrix formalism used to describe electron impact induced $np\leftrightarrow n's$ atomic transitions to include explicitly the effects of electron spin exchange. A general expression (24) for the scattering intensity was found which separates very clearly the dynamics of electron scattering from the geometric details of the initial state preparation and experimental geometry. Specific experiments were discussed which together can completely determine all of the complex scattering amplitudes describing this process except one phase difference between singlet and triplet amplitudes, and, of course, the overall arbitrary phase. For purposes of illustration, the experimental data of [11, 12] were recast in the form detailed in the present work and compared with the results of ab initio scattering calculations [20, 21]. At lower energies, about 2.0 eV, the 4-state close-coupling calculation [20] was found generally to be in quite reasonable agreement with the experiment. At higher energies, around 10.0 eV, the DWPO [21] was found to miss many of the essential details of the scattering process.

A complete characterization of this scattering process still requires a determination of the relative phase difference (δ^{st}, discussed in Sect. 4e) between singlet and triplet scattering. That requires a detailed analysis, analogous to that given in the present work, of experiments employing both preparation of the initial state and analysis of the final state. The relevant experimental data is not, at present, available, and that analysis is left for the future.

Appendix

In this appendix we discuss how the matrix elements $\sigma_{M_J M_J'}$ of the natural frame atomic preparation matrix (expressed in the $|JM_J\rangle$ basis) are obtained from a description, in the photon frame, of the atom prepared in a single hyperfine state. The formalism used here is discussed in several textbooks and articles, notably Brink and Satchler [33], Edmonds [34], Fano and Racah [35], Macek and Hertel [16], Hertel and Stoll [3], or Fischer and Hertel [27]. We take as the starting point of our derivation the density matrix elements $\sigma_{M_F M_F'}$ in the $|FM_F\rangle$ basis, given in the photon frame. We then construct multipole moments out of these, and project these moments onto the $|JM_J\rangle$ basis. Rotation into the natural frame is then performed, and real multipole moments are made from the complex ones. Finally, the elements $\sigma_{M_J M_J'}$ are extracted from these real multipole moments in the natural frame.

The multipole moments used in the present treatment are those constructed from angular momentum operators, and are referred to with the symbol $S_Q^K(F)$. These multipoles are equivalent to the $\langle T_q^k(ph)\rangle$ of Hertel and Stoll [3] and are related to the density matrix elements via the relations

$$S_Q^K(F)=\frac{1}{v^K(F)}\sum_{M_F M_F'}(-1)^{K-F-M_F}\cdot\langle KQ|F-M_F\,FM_F'\rangle\,\sigma_{M_F M_F'}, \tag{A1a}$$

$$\sigma_{M_F M_F'}=v^K(F)\sum_{QK}(-1)^{F-K+M_F}\cdot\langle F-M_F\,FM_F'|KQ\rangle\,S_Q^K(F), \tag{A1b}$$

where $v^K(F)$ is the ratio of the state multipoles to the multipole moments, and is given by

$$v^K(j)=\frac{2^K(2K+1)^{\frac{1}{2}}}{K!}(-1)^{2j}\left[\frac{(2j-K)!}{(2j+K+1)!}\right]^{\frac{1}{2}} \tag{A2}$$

with $j=F$ in our case. The multipole moments $S_Q^K(F)$ can be projected onto the $|JM_J\rangle$ basis as outlined in [27]:

$$S_Q^K(J)=\frac{v^K(F)}{v^K(J)}(2F+1)\begin{Bmatrix}F & F & K\\ J & J & I\end{Bmatrix}(-1)^{F+J-I+K}S_Q^K(F). \tag{A3}$$

Now we must rotate into the natural frame, which is accomplished with rotation matrices $D^K_{Q'Q}(\alpha\beta\gamma)$, as defined in [33]:

$$S_Q^K(\text{nat})=\sum_{Q'}S_{Q'}^K(\text{photon})\,D^K_{Q'Q}(\alpha\beta\gamma), \tag{A4}$$

where α, β and γ are the Euler angles used in rotating the photon frame axes into the natural frame axes. The natural frame multipole moments are then converted to real multipole moments $S^K_{0+}(\text{nat})$, $S^K_{Q+}(\text{nat})$, and $S^K_{Q-}(\text{nat})$ by the relations

$$S^K_{0+}(\text{nat})=S^K_0(\text{nat}), \tag{A5a}$$

$$S^K_{Q+}(\text{nat})=\frac{1}{\sqrt{2}}[S^K_{-Q}(\text{nat})+(-1)^Q S^K_Q(\text{nat}) +(-1)^Q S^K_Q(\text{nat})], \tag{A5b}$$

$$S^K_{Q-}(\text{nat})=\frac{i}{\sqrt{2}}[S^K_{-Q}(\text{nat})-(-1)^Q S^K_Q(\text{nat})]. \tag{A5c}$$

The final step is to express the matrix elements $\sigma_{M_JM'_J}$ in terms of the natural frame real multipole moments given in (A5a–c). This is done with (A1b), replacing F with J, and using (A5a–c) when necessary. The resulting explicit expressions for the elements of $\sigma_{M_JM'_J}$ are given below. We write down only the 10 elements of the upper right half of the 4×4 matrix, as the rest can be obtained from the fact that the matrix is Hermitian. Note that the multipole moments in these expressions are in the natural frame, although we drop the "(nat)" designation to simplify the notation.

$$\sigma_{\frac32,\frac32}=\frac14+\frac{3}{10}S^1_{0+}+\frac{1}{12}S^2_{0+}+\frac{1}{90}S^3_{0+}, \tag{A6a}$$

$$\sigma_{\frac32,\frac12}=\frac{\sqrt3}{10}(S^1_{1+}-iS^1_{1-})+\frac{1}{12}(S^2_{1-}-iS^2_{1-}) +\frac{1}{45\sqrt2}(S^3_{1+}-iS^3_{1-}), \tag{A6b}$$

$$\sigma_{\frac32,-\frac12}=\frac{1}{12}(S^2_{2+}-iS^2_{2-})+\frac{1}{18\sqrt5}(S^3_{2+}-iS^3_{2-}), \tag{A6c}$$

$$\sigma_{\frac32,-\frac32}=\frac{1}{9\sqrt{10}}(S^3_{3+}-iS^3_{3-}), \tag{A6d}$$

$$\sigma_{\frac12,\frac12}=\frac14+\frac{1}{10}S^1_{0+}-\frac{1}{12}S^2_{0+}-\frac{1}{30}S^3_{0+}, \tag{A6e}$$

$$\sigma_{\frac12,-\frac12}=\frac15(S^1_{1+}-iS^1_{1-})-\frac{1}{45}\sqrt{\frac32}(S^3_{1+}-iS^3_{1-}), \tag{A6f}$$

$$\sigma_{\frac12,-\frac32}=\frac{1}{12}(S^2_{2+}-iS^2_{2-})-\frac{1}{18\sqrt5}(S^3_{2+}-iS^3_{2-}), \tag{A6g}$$

$$\sigma_{-\frac12,-\frac12}=\frac14-\frac{1}{10}S^1_{0+}-\frac{1}{12}S^2_{0+}+\frac{1}{30}S^3_{0+}, \tag{A6h}$$

$$\sigma_{-\frac12,-\frac32}=\frac{\sqrt3}{10}(S^1_{1+}-iS^1_{1-})-\frac{1}{12}(S^2_{1+}-iS^2_{1-}) +\frac{1}{45\sqrt2}(S^3_{1+}-iS^3_{1-}), \tag{A6i}$$

$$\sigma_{-\frac32,-\frac32}=\frac14-\frac{3}{10}S^1_{0+}+\frac{1}{12}S^2_{0+}-\frac{1}{90}S^3_{0+} \tag{A6j}$$

(note that we have used the fact that $S^0_{0+}=1$ and $\sum_{M_J}\sigma_{M_JM_J}=1$ in the above).

Let us discuss how the relations outlined in this Appendix might actually be used in practice. If, as is often the case, the optical pumping is performed with pure linear or circular polarization, the density matrix $\sigma_{M_FM'_F}$ becomes diagonal in the photon frame [27]. Then from (A1a) we see that the only nonzero multipole moments are those with $Q=0$. The optically pumped atom can then be described in the $|JM_J\rangle$ basis by only three parameters (recall $J=3/2$, so $K_{\max}=3$):

$$S^1_0(J)=o_0(J)\quad\text{(orientation)}, \tag{A7a}$$

$$S^2_0(J)=a_0(J)\quad\text{(alignment)}, \tag{A7b}$$

$$S^3_0(J)=e_0(J)\quad\text{(octopole moment)}. \tag{A7c}$$

Furthermore, if steady state conditions are reached, circular polarization results in the $|FM_F\rangle$ density matrix element $\sigma_{3,3}$ (for left-handed polarization) or $\sigma_{-3,-3}$ (for right-handed polarization) being equal to unity while all other elements are zero. This leads to the values

$$o_0(J)=\pm3/2, \tag{A8a}$$

$$a_0(J)=3, \tag{A8b}$$

$$e_0(J)=\pm9/2. \tag{A8c}$$

where the + is for left-handed polarization and the − is for right-handed polarization. Steady state pumping with linearly polarized light creates the values $\sigma_{0,0}=\frac{10}{21}$, $\sigma_{1,1}=\sigma_{-1,-1}=\frac{5}{21}$ and $\sigma_{2,2}=\sigma_{-2,-2}=\frac{1}{42}$ [3, 27], and all other elements equal to zero. This results in

$$o_0=0 \tag{A9a}$$

$$a_0=-2, \tag{A9b}$$

$$e_0=0. \tag{A9c}$$

In principle, the numbers o_0, a_0 and e_0 can be measured without too much difficulty, so the values in (A 8) and (A 9) could be corrected to reflect real conditions if necessary. However for practical purposes at not too high atom beam densities ($<10^{10}$ cm^{-3}), well collimated beams, low magnetic fields (<5 mg), and not too high laser intensities (<100 mW/cm^2), one may safely assume stationary conditions.

Having only $Q=0$ multipoles in the photon frame allows the rotation into the natural frame to be carried out very simply, because the rotation matrices $D^K_{Q0}(\alpha\beta\gamma)$ can be expressed in terms of modified spherical harmonics C_{KQ}. The resulting expressions for the real multipole moments in the natural frame are

$$S^K_0(\text{nat}) = S^K_0(\text{photon})\, C_{K0}(\theta, \varphi), \tag{A 10a}$$

$$S^K_{Q+}(\text{nat}) = S^K_0(\text{photon})\,(-1)^Q \sqrt{2}\,\text{Re}[C_{KQ}(\theta, \varphi)], \tag{A 10b}$$

$$S^K_Q(\text{nat}) = S^K_0(\text{photon})\,(-1)^Q \sqrt{2}\,\text{Im}[C_{KQ}(\theta, \varphi)], \tag{A 10c}$$

where, as shown in Fig. 8, θ and φ are the polar angles describing the direction of $\hat{\mathbf{z}}_{\text{photon}}$ with respect to $\hat{\mathbf{z}}_{\text{nat}}$. Thus if pure linear or circular polarization is used and steady state conditions exist, one need only take the values given in (A 8 a–c) or (A 9 a–c), rotate these with (A 10 a–c) and insert the results into (A 6 a–j). This is the procedure used in Sect. 4. Usually some care is advisable when defining the angles θ and φ and the exact orientation of the natural reference frame, as discussed in Sect. 3 a. A detailed discussion of an example is given in Sect. 5 b.

In the most general case, when, for example, elliptically polarized light is used and/or non-steady-state conditions exist, the most practical approach would probably be to perform an ab initio calculation of the density matrix elements $\sigma_{M_F M'_F}$. Then (A 1–A 6) would have to be used in their most general form.

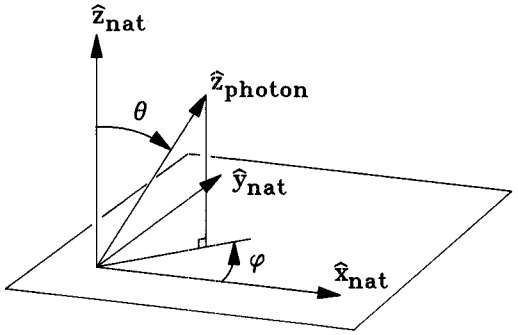

Fig. 8. Definition of the angles θ and φ describing the direction of $\hat{\mathbf{z}}_{\text{photon}}$ with respect to the natural frame

Rather complicated expressions for the elements $\sigma_{M_J M'_J}$ would most likely arise, but in principle their application to the problem would be straightforward.

References

1. For a recent review see, e.g., Slevin, J.: Rep. Prog. Phys. **47**, 461 (1984); For a comprehensive survey currently under preparation, see Andersen, N., Gallagher, J.W., Hertel, I.V.: Phys. Rep. (to be published)
2. The pioneering experiments for this technique were performed by Eminyan, M., MacAdam, K.B., Slevin, J., Kleinpoppen, H.: J. Phys. B**7**, 1519 (1974)
3. The first experiments of this kind were performed by Hertel, I.V., Stoll, W.: J. Phys. B**7**, 583 (1974); For a review see Hertel, I.V., Stoll, W.: At. Mol. Phys. **13**, 113 (1977)
4. For a discussion and further references see, e.g., Andersen, N., Hertel, I.V.: Comm. Atom. Mol. Phys. **19**, 1 (1986)
5. Callaway, J., McDowell, M.R.C.: Comm. Atom. Mol. Phys. **13**, 19 (1983)
6. A review of recent work involving spin-polarization studies is given by Hanne, G.F.: Phys. Rep. **95**, 95 (1983)
7. The standard textbook for spin-polarized electrons is Kessler, J.: Polarized electrons, 2nd ed. New York, Berlin: Springer-Verlag 1985
8. Bederson, B.: Comm. Atom. Mol. Phys. **1**, 41 (1971); ibid. **1**, 65 (1971); ibid. **2**, 160 (1971)
9. Goeke, J., Hanne, G.F., Kessler, J., Wolcke, A.: Phys. Rev. Lett. **51**, 2273 (1983)
10. Hanne, G.F., Szmytkowski, Cz., van der Wiel, M.: J. Phys. B**15**, L109 (1982)
11. McClelland, J.J., Kelley, M.H., Celotta, R.J.: Phys. Rev. Lett. **55**, 688 (1985)
12. McClelland, J.J., Kelley, M.H., Celotta, R.J.: Phys. Rev. Lett. **56**, 1362 (1986)
13. Hermann, H.W., Hertel, I.V.: Z. Phys. A – Atoms and Nuclei **307**, 89 (1982)
14. Also coincidence experiments have been peformed for this system, see: Riley, J.L., Teubner, P.J.O., Brunger, M.J.: Phys. Rev. A**31**, 1959 (1985);
    Teubner, P.J.O., Riley, J.L., Furst, J.E., Buckman, S.J.: J. Phys. B**18**, 351 (1985);
    Riley, J.L., Teubner, P.J.O., Brunger, M.J.: J. Phys. B**19**, 129 (1986)
15. Fano, U., Macek, J.H.: Rev. Mod. Phys. **45**, 553 (1973)
16. Macek, J.H., Hertel, I.V.: J. Phys. B**7**, 2173 (1974)
17. Hermann, H.W., Hertel, I.V.: Comm. Atom. Mol. Phys. **12**, 61 (1982); ibid. **12**, 127 (1982)
18. Andersen, N., Hertel, I.V., Kleinpoppen, H.: J. Phys. B**17**, L901 (1984)
19. Andersen, N., Gallagher, J.W., Hertel, I.V.: In: Electronic and atomic collisions, Proceedings of the XIV$^{\text{th}}$ ICPEAC. Lorents, D.C., Meyerhof, W.E., Peterson, J.R. (eds.), p. 57. Amsterdam, Oxford, New York, Tokyo: North Holland 1986
20. Moores, D.L., Norcross, D.W., J. Phys. B**5**, 1482 (1972)
21. Kennedy, J.V., Myerscough, V.P., McDowell, M.R.C.: J. Phys. B**10**, 3759 (1977)
22. Newton, R.G.: Scattering theory of waves and particles, 2nd Edn. Berlin, Heidelberg, New York: Springer 1982
23. Macek, J.H.: In: Fundamental processes in energetic collisions. Lutz, H.O., Briggs, J.S., Kleinpoppen, H. (eds.), p. 39. New York, London: Plenum Press 1982
24. Blum, K.: Density matrix theory and applications. New York, London: Plenum Press 1981

25. Blum, K., Kleinpoppen, H.: Phys. Rev. **52**, 203 (1979)
26. Percival, I.C., Seaton, M.J.: Philos. Trans. R. Soc. London A **251**, 113 (1958)
27. Fischer, A., Hertel, I.V.: Z. Phys. A – Atoms and Nuclei **304**, 103 (1982)
28. Hanne, G.F.: Comm. At. Mol. Phys. **14**, 163 (1984)
29. Csanak, G., Cartwright, D.C.: J. Phys. B **19**, L485 (1986)
30. Andersen, N., Andersen, T., Dahler, J.S., Nielsen, S.E., Nienhuis, G., Refsgaard, K.: J. Phys. B **16**, 817 (1983)
31. Neitzke, H.-P., Andersen, T.: J. Phys. B **17**, 1559 (1984)
32. Pierce, R.J., Celotta, R.J., Wang, G.-C., Unertl, W.N., Galejs, A., Kuyatt, C.E., Mielczarek, S.R.: Rev. Sci. Instrum. **51**, 478 (1980)
33. Brink, D.M., Satchler, G.R.: Angular momentum, 2nd Edn. Oxford: Clarendon Press 1968
34. Edmonds, A.R.: Angular momentum in quantum mechanics, 2. Edn. Princeton: Princeton University Press 1960
35. Fano, U., Racah, G.: Irreducible tensorial sets. New York: Academic Press 1959

I.V. Hertel
Fakultät für Physik
Universität Freiburg
Hermann-Herder-Strasse 3
D-7800 Freiburg im Breisgau
Federal Republic of Germany

M.H. Kelley, J.J. McClelland
Radiation Physics Division
National Bureau of Standards
Gaithersburg, MD 20899
USA